



TECHNISCHE  
UNIVERSITÄT  
WIEN  
Vienna University of Technology

## **DIPLOMARBEIT**

### **Adaptive Optics Scanning Laser Ophthalmoscope**

Ausgeführt am

**Institut für Angewandte Physik  
der Technischen Universität Wien**

unter der Anleitung von

**Ao.Univ.Prof. Dipl.-Ing. Dr.techn. Martin Gröschl**

in Zusammenarbeit mit

**Assoc. Prof. Priv.-Doz. Dipl.-Ing. Dr. Michael Pircher**

**Zentrum für Medizinische Physik und Biomedizinische Technik  
der Medizinischen Universität Wien**

durch

**Gerold Christian Aschinger**

Austinstraße 50, 3107 St. Pölten

9. September 2012

# Acknowledgements

At first I want to thank Prof. Michael Pircher from the Center for Medical Physics and Biomedical Engineering at the Medical University of Vienna for giving me the opportunity to be part of his group and supporting me at my work. I also want to express special thanks to DI Franz Felberer. He was always a helpful co-worker and I benefited much from his experience in the field of work. I appreciated the teamwork and the good working atmosphere in the group.

Furthermore I want to thank Prof. Martin Gröschl from the Vienna University of Technology for giving me the chance to do my Master thesis at the Medical University of Vienna and introducing me to Prof. Pircher. I also want to thank him for his support during my work. Thanks to the Vienna University of Technology and the Institute of Applied Physics.

I also want to thank the many colleagues I have met at the Center for Medical Physics and Biomedical Engineering for their friendly welcome and their support. Especially, I would like to thank the members of the mechanical workshop.

Thanks to the Austrian Science Fund (FWF project P22329-N20) for supporting me financially during my work.

And most of all, I thank my parents Renate and Hubert Aschinger, my sister Verena Aschinger-Huber and my brother Roland Aschinger for always supporting me and encouraging me in my ambitions.

# Contents

<b>1</b>	<b>Introduction and motivation</b>	<b>1</b>
<b>2</b>	<b>Method</b>	<b>4</b>
2.1	Scanning laser ophthalmoscope . . . . .	4
2.2	Adaptive optics . . . . .	5
2.2.1	Wave front detection . . . . .	6
2.2.2	Wave front correction . . . . .	7
2.2.3	AO software . . . . .	8
2.3	Lens based SLO . . . . .	8
2.4	Alignment method . . . . .	9
2.4.1	Imaging of the wave front . . . . .	9
2.4.2	Imaging of the retina . . . . .	9
2.4.3	Adapting of beam diameter . . . . .	10
2.5	Alignment of the telescopes . . . . .	11
2.6	Signal to noise ratio . . . . .	12
2.7	Laser safety . . . . .	12
<b>3</b>	<b>Experimental setup</b>	<b>14</b>
3.1	Components . . . . .	15
3.1.1	Light source . . . . .	15
3.1.2	Shack-Hartmann wave front sensor . . . . .	16
3.1.3	Deformable mirror . . . . .	18
3.1.4	Resonant scanner . . . . .	20
3.1.5	Galvo scanner . . . . .	21
3.1.6	Avalanche photo diode . . . . .	22
3.1.7	Data acquisition board . . . . .	22
3.1.8	Lenses . . . . .	22
3.2	Beam propagation . . . . .	23
3.2.1	Beam diameter . . . . .	23
3.2.2	Light path . . . . .	23

<b>4</b>	<b>System alignment</b>	<b>27</b>
4.1	Prearrangements . . . . .	27
4.1.1	Collimator alignment . . . . .	27
4.1.2	Determination of the setup height . . . . .	29
4.2	Adjusting the entrance collimator . . . . .	29
4.3	Alignment of SH-sensor to entrance collimator . . . . .	30
4.4	Alignment of first lens to SH-sensor . . . . .	32
4.5	Alignment of first telescope and aperture . . . . .	34
4.6	Alignment of the Galvo scanner . . . . .	36
4.7	Alignment of the second telescope . . . . .	39
4.8	Alignment of the third telescope and the deformable mirror . .	41
4.9	Alignment of the fourth telescope and the Badal system . . . .	45
4.10	Alignment of the detector collimator . . . . .	46
4.11	Problems with the alignment . . . . .	48
<b>5</b>	<b>Adaptive optics loop control using Matlab</b>	<b>49</b>
5.1	Introduction . . . . .	49
5.2	Prearrangements . . . . .	49
5.3	Closed loop control . . . . .	52
<b>6</b>	<b>System characterization and measurements</b>	<b>56</b>
6.1	Rough calculation of the required sensitivity of the SH-sensor for in vivo measurements . . . . .	56
6.2	Measurement of the system sensitivity . . . . .	57
6.3	Artificial eye and in vivo imaging of a human eye . . . . .	58
<b>7</b>	<b>Discussion and outlook</b>	<b>64</b>
<b>A</b>	<b>Matlab scripts</b>	<b>69</b>
A.1	userStartup . . . . .	69
A.2	LOOPScript . . . . .	70
A.3	LoadIMScript . . . . .	71



Table 1: Abbreviations used in the thesis.

A	Aperture
ACE	Alpao Core Engine
AE	Artificial eye
AMD	Age-related macular degeneration
AO	Adaptive optics
AO-SLO	Adaptive optics scanning laser ophthalmoscope
APD	Avalanche photo diode
C	Collimator
DAQ	Data acquisition
DC	Detector collimator
DIT	Data integration time
DM	Deformable mirror
EC	Entrance collimator
EL	Eye lens
ELS	External light source
F	Fovea
FFT	Fast Fourier transform
FPGA	Field-programmable gate array
G	Glass-body
GS	Galvo scanner
IM	Interaction matrix
L	Lens
M	Mirror
O	Observer
OCT	Optical coherence tomography
P	Pellicle
P1, P2	Polarizer1, Polarizer2
PBS	Polarizing beam splitter
PV	Peak-to-valley
QWP	Quarter-wave plate
R	Retina
RMS	Root mean square
RS	Resonant scanner
SH	Shack-Hartmann
SLD	Superluminescent diode
SLO	Scanning laser ophthalmoscope
SM	Single mode
SNR	Signal-to-noise ratio
WFS	Wave front sensor

# Chapter 1

## Introduction and motivation

The eye is a very important sensory organ for humans. Without the capability to see a human being's daily routine changes dramatically. Mankind developed various optical aids to correct defective vision arising from imaging errors, like spectacles, or to improve vision, like telescopes. However, there are many reasons for defective vision not originating from imaging problems of the eye but arising from retinal diseases like age-related macular degeneration (AMD) [1–3] or retinal dystrophies [1, 3–5]. In order to provide improved diagnosis and treatment detailed and accurate information on disease related changes of the retina is required.

The retina is the actual light sensing part of the eye, which also preprocesses the information provided by the measured light for final processing in the brain [6]. Figure 1.1 shows a schematic of the human eye and Fig. 1.2 shows the different layers of the retina without going into detail of the function of each layer. The retina is a neural tissue at the back of the eye [6]. When light hits the retina an electrical signal is generated within the photoreceptor's outer segments (c.f. Fig. 1.2) and transmitted to the brain [6]. The sensor elements (photoreceptors) of the retina can be divided into cones and rods [6]. Cones are responsible for daylight and color vision [6]. There is only a small area on the retina which enables humans to see detailed, sharp color images. This area is called the fovea and is located in the foveal pit [6]. The fovea is the area with the highest photoreceptor density and the least vessel density of the retina [6]. There are three different types of cones, each type sensitive for different wavelength regions (long (L)/middle (M)/short (S) wavelength sensitivity ranging from red to blue) [6]. L and M cones are most densely packed in the fovea (spacing about 1-2  $\mu\text{m}$ ) [6]. With increasing distance from the fovea their diameter increases to 4 or 5  $\mu\text{m}$  with decreasing packing density [6]. Rods are mainly responsible for vision in dim illumination [6].

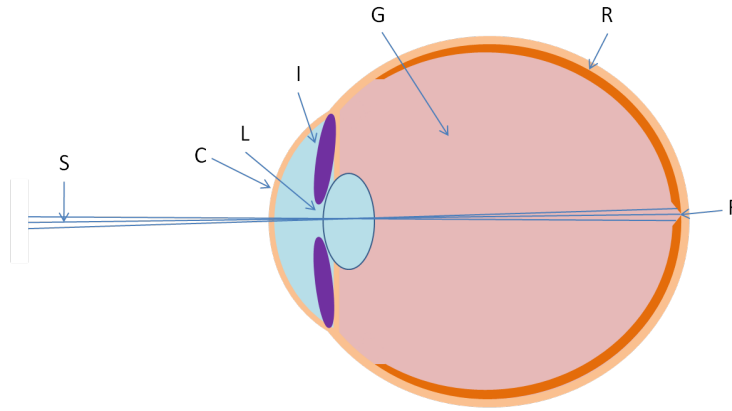


Figure 1.1: Schematic of the human eye. C...cornea, L...eye lens, I...iris, G...glass-body, R...retina, F...fovea, S...sight-axis. Adapted from [3]

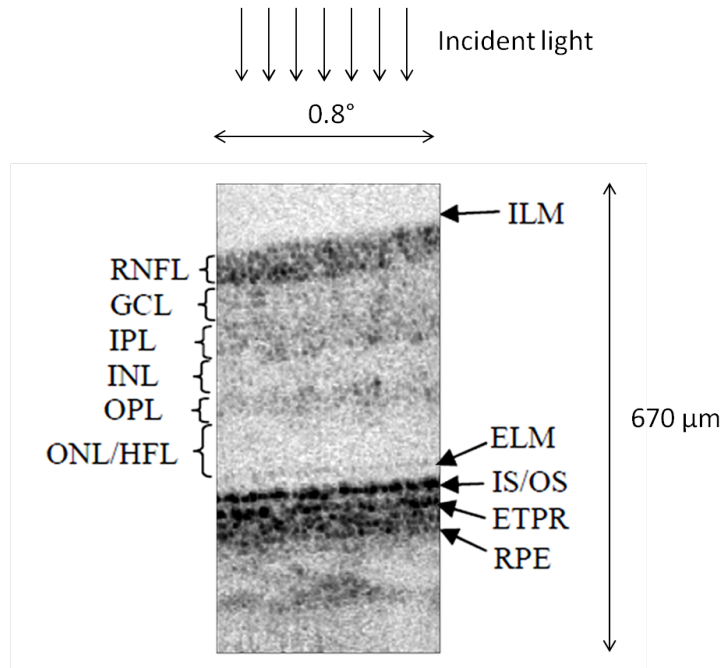


Figure 1.2: Different layers of the retina imaged in vivo with a high resolution OCT-system. ILM...inner limiting membran, RNFL...retinal nerve fiber layer, GCL...ganglion cell layer, IPL...inner plexiform layer, INL...inner nuclear layer, OPL...outer plexiform layer, ONL/HFL...outer nuclear layer/Henle fiber layer, ELM external limiting membrane, IS/OS...junction between inner and outer segments of photoreceptors, ETPR...end tips of photoreceptors, RPE...retinal pigment epithelium. Adapted from [7].

In vivo imaging of the human retina on a cellular level is challenging because of the limited optical aperture of the eye, the weakly backscattering structures [8] and the rapid eye motion [7]. Retinal diseases alter the normal retinal structures, however, the pathogenesis of many diseases of the retina is still unclear [1, 2]. High resolution imaging of the retina is necessary in order to detect early changes in the retina on a cellular level due to disease [7]. Clinically established methods like direct funduscopy [9], fundus photography [9], scanning laser ophthalmoscopy (SLO) [10] or optical coherence tomography (OCT) [11, 12] do not provide cellular resolution. This is mainly caused by imperfections of the human eye optics (cornea, lens; c.f. Fig. 1.1) which prevents imaging with diffraction limited resolution at the highest possible magnification [13]. To elevate this limitation these aberrations have to be corrected [14–16]. One possibility is the use of adaptive optics (AO), where the wave front exiting the eye is measured constantly and the detected aberrations are corrected with a correcting device [8]. AO can be combined with all previously mentioned imaging techniques. However, this work focuses on the SLO technique. This technique uses a laser to illuminate the retina while the laser beam is scanned in x- and y- direction. The back scattered light at each position is measured and the information can be translated into a two dimensional image of the scanned area. Up to now adaptive optics scanning laser ophthalmoscopy (AO-SLO) enabled imaging of small structures (e.g. cones and rods) in unprecedented quality [14, 17].

This master thesis deals with the implementation of a lens based AO-SLO [14]. In comparison to the state of the art approach using spherical mirrors for imaging [17, 18] the described setup uses lenses for imaging. The main objective is to build a more compact design (in comparison to [14]) and to implement a new deformable mirror in combination with a high resolution wave front sensor. One part of the thesis covers the alignment of the setup which is a very difficult task that requires high accuracy. Further parts cover the setup characteristics and the description of the software to drive the AO-system. In the last part measurements in a model eye and in vivo measurements of a healthy human volunteer are shown.

# Chapter 2

## Method

This chapter gives insight in the main methods used for the experimental setup. At first the SLO technique will be described. After that the principles of adaptive optics and the devices and methods to correct wave front aberrations will be explained.

### 2.1 Scanning laser ophthalmoscope[10]

The principle of the scanning laser ophthalmoscope (SLO) is to illuminate the retina with a scanning laser beam and measure the backscattered light at each location. To get a two dimensional image of the retina, it is scanned e.g. line by line. This can be achieved by two scanners. The faster scanner scans the rows and whenever a row is finished the slower scanner changes its scanning angle to the next line. In order to focus the beam on the retina the eye is illuminated with a collimated beam (c.f. Fig. 2.1, emmetropic eye).

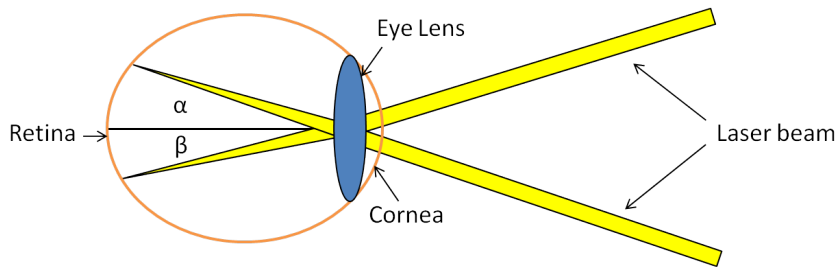


Figure 2.1: Two different scanning angles  $\alpha, \beta$  on the retina. The scanning angle on the retina is proportional to the scanning angle of the scanner.

The position of that illuminated point depends on the current angle of the scanner heads. The light is backscattered from the tissue in the retina and

the amount of the backscattered intensity gives insight into the underlying tissue at that point. This backscattered light travels back through the SLO setup and is measured with a very sensitive detector (e.g. an avalanche photo diode (APD)). The signal from the detector is recorded with a data acquisition board and translated into an image.

## 2.2 Adaptive optics [19]

Adaptive optics (AO) is a technique to correct wave front distortions[19]. It is for instance used in astronomy for ground based telescopes to adjust wave front deformations[19]. If the plane wave from a star enters the earth's atmosphere different layers of the atmosphere cause different indices of refraction and distort the wave front[19]. This makes sharp diffraction limited images of the star impossible[19]. To elevate this limitation one can use AO[19]. With a wave front sensor the deformations of the wave front are measured and can be corrected with e.g. a deformable mirror [19] (c.f. Fig. 2.2).

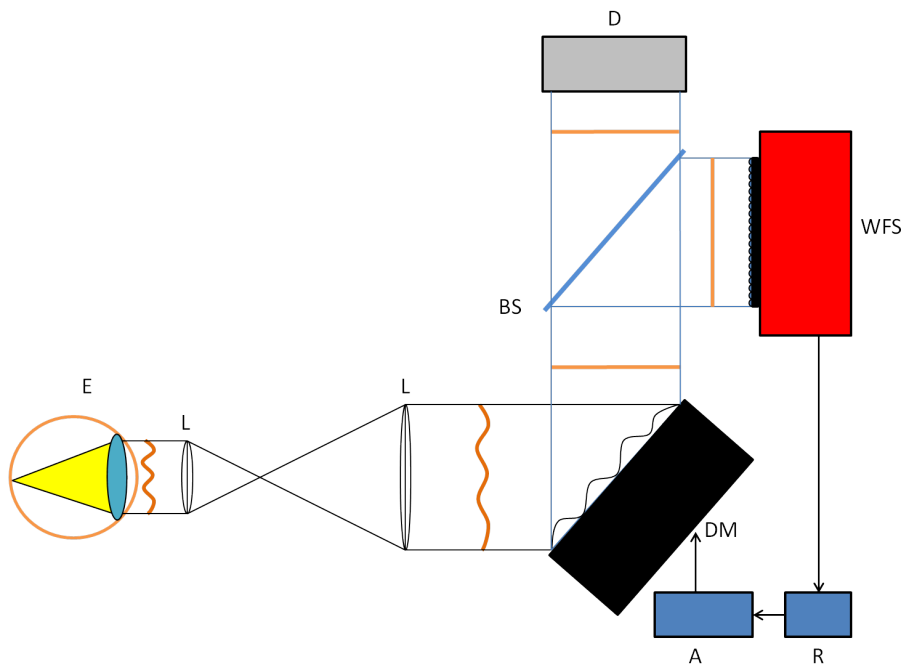


Figure 2.2: Basic scheme of an AO system for ophthalmology. D...Detector and light source, WFS...wave front sensor, DM...deformable mirror, BS...beam splitter, L...lenses, E...eye, R...wave front reconstructor, A...actuator control. Adapted from [20].

### 2.2.1 Wave front detection[21]

To detect wave front distortions a Shack-Hartmann (SH) wave front sensor can be used. This wave front sensor consists of a lenslet array mounted in front of a charge coupled device (CCD) or a complementary metal-oxide semiconductor (CMOS) area detector [21]. The detector is placed in the focal plane of the lenslet array. If a plane wave is measured, every micro lens projects the parallel light into its focal point, which is exactly where the optical axis of each micro lens intersects the sensor chip, see Fig. 2.3.

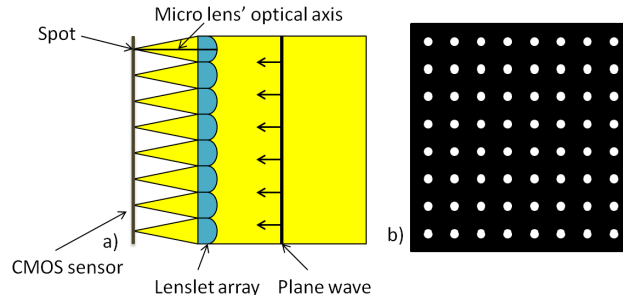


Figure 2.3: Measuring a plane wave with a SH wave front sensor. a) Schematic of the SH-sensor, b) Detected spot pattern. Adapted from [21]

If a distorted wave front hits the wave front sensor the micro lenses won't project the light on the point where the optical axis intersects the sensor plane.

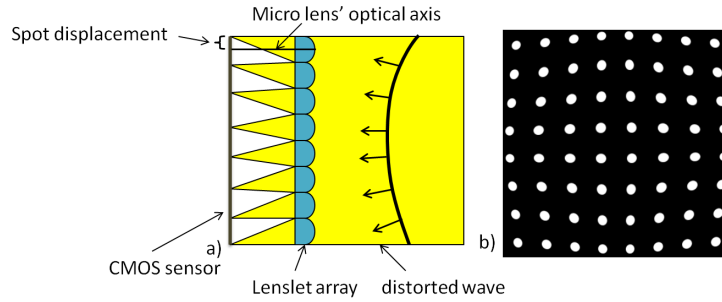


Figure 2.4: Measuring a distorted wave front with a SH-sensor. The focal spots are no longer at the optical axis of each micro lens. a) Schematic of the SH-sensor, b) Detected spot pattern. Adapted from [21]

Now the spots will be at different positions as shown in Fig. 2.4. The spot displacement is proportional to the slopes of the wave front [21]. The

spots can be found with a spot finding algorithm and the wave front x- and y-slopes can be computed out of the two dimensional spot pattern with Eq. 2.1 and Eq. 2.2 [21].

$$\frac{\partial W(x, y)}{\partial x} = \frac{\Delta x_s}{F} \quad (2.1)$$

$$\frac{\partial W(x, y)}{\partial y} = \frac{\Delta y_s}{F} \quad (2.2)$$

$W(x, y)$  is the original wave front,  $\Delta x_s$  and  $\Delta y_s$  are the spot displacements in x and y direction and  $F$  is the focal length of the micro lenses. The local wave front slopes allow reconstructing the wave front (c.f. Fig. 2.5) via integration [21].

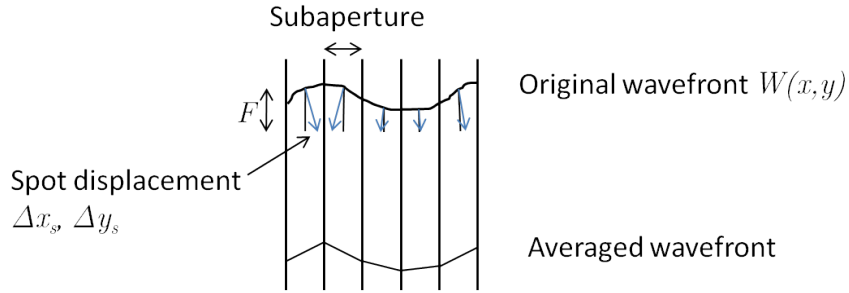


Figure 2.5: Measuring the local slopes of the wave front with a SH-sensor. Adapted from [21].

The spatial resolution of the measured wave front corresponds to the distance between the lenslets. Sometimes it is helpful to approximate the wave front with the use of Zernike polynomials. The different Zernike polynomials can be assigned to wave front aberrations like e.g. defocus [22]. The first nine Zernike polynomials and the associated wave front aberrations are shown in Tab. 2.1. From the reconstructed wave front the Zernike coefficients are calculated [21, 22].

### 2.2.2 Wave front correction

When the wave front deformations are known they need to be corrected with e.g. a deformable mirror (DM). One possible way to implement a DM is a reflecting membrane with several actuator elements behind the membrane [23] (another possible wave front correction device is a microelectromechanical system (MEMS) mirror[24]). These elements can be controlled independently. As a consequence the mirror can be given various shapes. With the



measured wave front aberrations the shape for the DM to correct these aberrations can be calculated and set. Usually the SH wave front sensor and the DM are driven in closed loop mode (see next chapter).

To check the wave front correction the change of the root mean square (RMS) wave front error of the corrected wave front is observed. The RMS for a wave front is calculated by the square root of the sum of the squared Zernike coefficients of the wave front [8].

### 2.2.3 AO software

The closed loop mode is an iterative algorithm which measures the wave front and applies a corresponding signal to the wave front correction device [25]. In each loop step the residual wave front error should get smaller (c.f. Fig. 2.6).

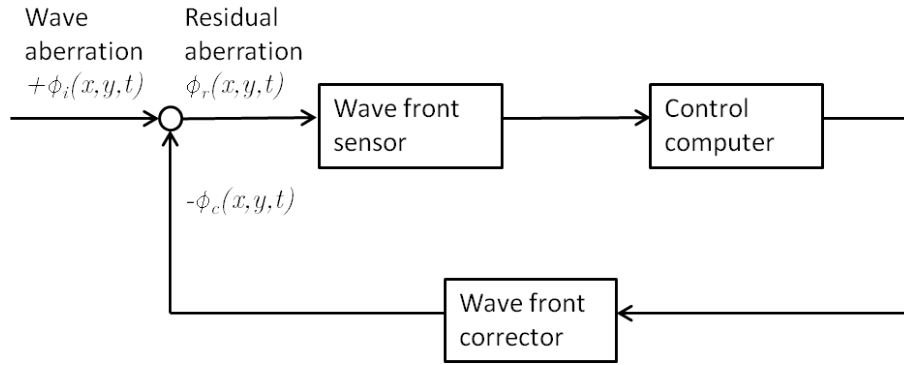


Figure 2.6: Control loop for closed loop operation. Adapted from [25].

The input function  $\phi_i(x, y, t)$  in Fig. 2.6 is the measured wave front aberration at the point (x,y) at time t.  $\phi_c(x, y, t)$  is the correction performed by the DM and  $\phi_r(x, y, t)$  is the residual wave front aberration at the same point and time [25]. The residual aberration after each loop step can be computed with Eq. 2.3[25].

$$\phi_r(x, y, t) = \phi_i(x, y, t) - \phi_c(x, y, t) \quad (2.3)$$

The loop is executed and  $\phi_r(x, y, t)$  should get smaller with each loop[25].

## 2.3 Lens based SLO

One advantage of the lens based approach in comparison to standard AO-SLO using spherical mirrors[15] is that less aberrations are introduced[14].

Therefore the aberrations introduced by the system itself are kept low[14]. Furthermore a lens based SLO can in principle be built more compact in a limited space since the folding of the light path necessary when using spherical mirrors for imaging [17] is avoided by using lenses for imaging[14]. Another advantage of the lens based SLO technique is that the light path remains in the same height for all telescopes[14]. For mirror based SLOs a three dimensional light path must be introduced to correct the astigmatism caused by the spherical mirrors[17]. This makes the alignment of such mirror based SLOs more difficult.

One problem of the lens based system are back reflections from the lens surfaces[14]. These reflections cause additional spots on the SH-sensor image and distort the wave front measurement[14]. To avoid this polarization optics are used[14].

## **2.4 Alignment method**

For the AO-SLO to work the following three requirements must be fulfilled.

### **2.4.1 Imaging of the wave front**

Since the SLO setup is enhanced with AO the wave front exiting the eye has to be imaged onto DM and SH-sensor, respectively. To achieve this telescopes (consisting of either spherical mirrors or lenses) are used. Wave front correction is only achieved if the imaging is rather perfect. Additionally, x-y scanners are used to create a 2D image of the retina. To avoid blurring of the wave front aberrations, the pivot points of the scanners have to be imaged onto DM and SH which requires additional telescopes between the elements. If the setup is misaligned and the DM is not imaged on the SH-sensor a good correction will not be possible. Therefore a minimum of four telescopes is required for an AO-system.

### **2.4.2 Imaging of the retina**

In addition to the wave front imaging, the retina has to be imaged onto the detector. This can be achieved in a similar way using telescopes. Note that in order to fulfil both imaging conditions, a single lens cannot be used for imaging.

### 2.4.3 Adapting of beam diameter

For the ideal system the beam diameter within the system matches the diameter of the dilated eye pupil ( $\sim 7$  mm). Since the SH-sensor and the DM in general have different diameters than this pupil the beam diameter must be adapted to exploit the full aperture of each element. The beam diameter after the entrance collimator was designed to match the aperture of the SH-sensor.

This diameter can be computed with the numerical aperture  $A_N = 0.1$  of the fiber connected to the collimator and the focal length of the collimator. With Eq. 2.4 the half angle of the cone  $\alpha_{max}$  exiting the fiber can be calculated [19].

$$A_N = \sin \alpha_{max} \quad (2.4)$$

With the collimator lens' focal length  $f$  the half beam diameter  $d$  can be calculated (c.f. Eq. 2.5).

$$\frac{d}{f} = \tan \alpha_{max} \quad (2.5)$$

To get the beam diameter  $d_b$  the focal length of the collimator lens  $f$  and  $\alpha_{max}$  must be inserted in Eq. 2.6.

$$d_b = 2f \tan \alpha_{max} \quad (2.6)$$

This yields the beam diameter after the entrance collimator. To increase the beam diameter lenses with different focal length can be introduced into the telescope as shown in Fig. 2.7.

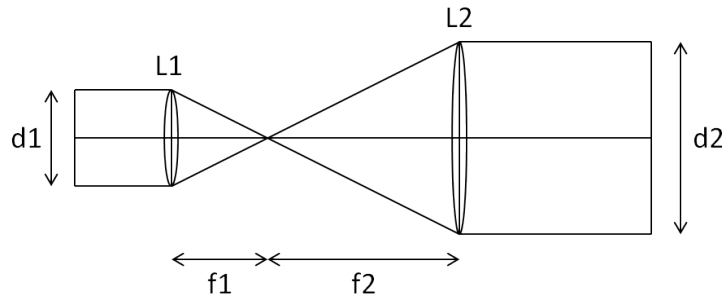


Figure 2.7: Change in beam diameter due to different focal lengths of the lenses in a telescope. L1, L2...lenses,  $f_1$ ,  $f_2$ ...focal lengths,  $d_1$ ,  $d_2$ ...beam diameters

The new beam diameter can be calculated with Eq. 2.7.

$$d_2 = \frac{f_2}{f_1} d_1 \quad (2.7)$$

Similarly the reduction of the beam diameter by a telescope can be calculated with Eq. 2.7. Since the diameter of SH-sensor, DM and the eye are fixed these three conditions already define the possible focal length ratios of each telescope.

## 2.5 Alignment of the telescopes

As described before imaging of the different planes (retina, pupil) is essential for AO. The idea is to use the SH-sensor itself as a very accurate instrument for system alignment. However, when aligning a telescope in a double pass configuration as will be described later on, an additional element is required to limit the possible light paths. Using a variable aperture set to the minimum diameter as additional reference allows the light only to travel along the optical axis of the telescope (c.f. Fig. 2.8).

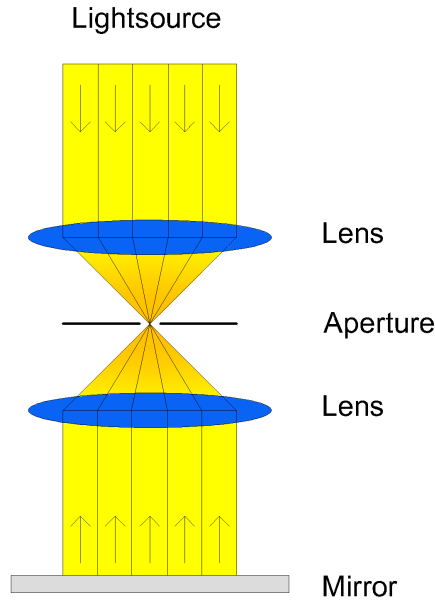


Figure 2.8: Telescope with aperture located in the focal point of both lenses. Only if the telescope is perfectly aligned the light will traverse the small aperture.

## 2.6 Signal to noise ratio

In addition to the sharpness the signal to noise ratio (SNR) of the system influences the imaging quality. It can be calculated from an image with Eq. 2.8, where  $S_{max}$  is the maximum signal in an image and  $\sigma$  is the standard deviation of the noise of the image.

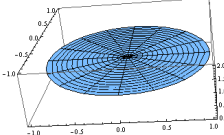
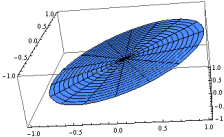
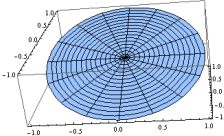
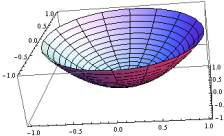
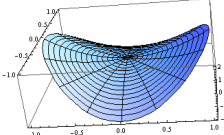
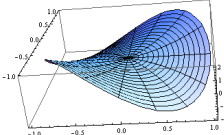
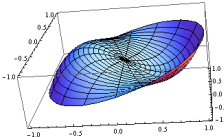
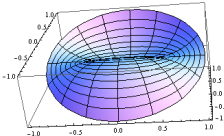
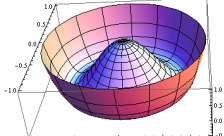
$$SNR = 10 \log \frac{S_{max}}{\sigma} [dB] \quad (2.8)$$

## 2.7 Laser safety

Laser safety is a very important issue when adjusting the setup or during measuring. In all situations the light power levels have to be kept below the limits provided by the laser safety guideline (EN-60825-1). For the used wavelength region (840 nm) thermal retinal damage may occur. Keeping the light power below 700  $\mu$ W at this wavelength region is regarded as safe for intra-beam viewing for more than 8 hours. In order to minimize possible risks, the light power is reduced during alignment. Additionally the light path is checked before the first switching on of the light source.

Before in vivo measurement with the SLO the power exiting the instrument has to be checked to be lower than 700  $\mu$ W.

Table 2.1: First nine Zernike polynomials (DIN/ISO) [22].  $\rho$  is the radius,  $\theta$  is the angle of the polar coordinate system.  $\rho$  can be between 0 and 1.

Zernike order	Zernike polynomial	Graphical representation	Name of aberration
0	1		Piston
1	$\rho \cos \theta$		Tip
2	$\rho \sin \theta$		Tilt
3	$(2\rho^2 - 1)$		Defocus
4	$2\rho^2 \cos 2\theta$		Astigmatism 0°, 1st
5	$2\rho^2 \sin 2\theta$		Astigmatism 45°, 1st
6	$(3\rho^3 - 2\rho) \cos \theta$		Coma x
7	$(3\rho^3 - 2\rho) \sin \theta$		Coma y
8	$(6\rho^4 - 6\rho^2 + 1)$		Spherical

# Chapter 3

## Experimental setup

Figure 3.1 shows the final setup of the lens based AO-SLO system. At first this chapter gives an insight in the different devices and the technical features used in the setup. In the second part the light path of the setup is explained.

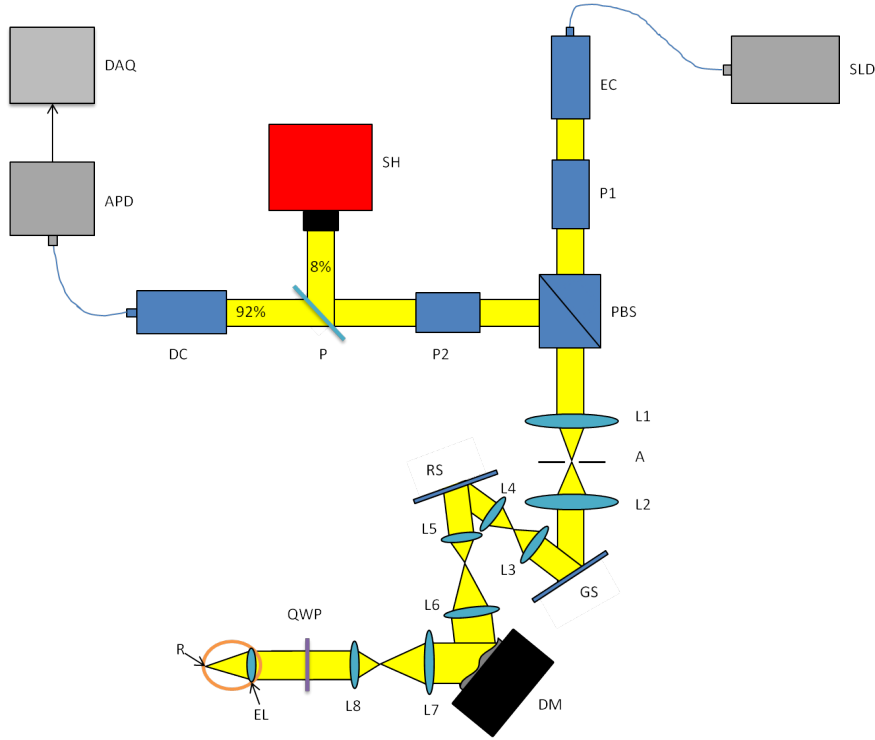


Figure 3.1: Scheme of the experimental setup. SH...SH wave front sensor, DM...deformable mirror, GS...Galvo scanner, RS...resonant scanner, SLD...superluminescent diode DAQ...data acquisition, APD...avalanche photo diode, EC...entrance collimator, DC...detector collimator, PBS...polarizing beam splitter, QWP...quater-wave plate, A...aperture, P...pellicle, R...retina, EL...eye lens, L1-L8...lenses

## 3.1 Components

### 3.1.1 Light source [26]

The setup's light source (Superlum SLD-371) is a superluminescent diode (SLD) with a central wavelength of 842.8 nm and a spectral width of 50.8 nm (full width at half maximum). Using a broad band light source reduces the effect of speckles[8]. The Superlum SLD-371 provides an output power of up to 20 mW.



### 3.1.2 Shack-Hartmann wave front sensor [27]

The Shack-Hartmann (SH)-sensor used for the adaptive optics setup is fabricated by Optocraft. It consists of a lenslet array with the characteristics shown in Tab. 3.1 and a Photonfocus CMOS sensor. The sensor chip has the characteristics shown in Tab. 3.2.

Table 3.1: Lenslet array characteristics. [27]

Type	Refractive
Wavelength / nm	840
Distance / mm	0.15
Focallength f / mm	4.306
Front surface	Plane surface
Masked subaperture	yes
Antireflection coating	yes
Distance from mounting flange to microlenses / mm	13.32

Table 3.2: Sensor chip characteristics. [27]

Type	Photonfocus MV1-D1312-C035-240-CL-8
Pixel size / $\mu\text{m}^2$	8.0 x 8.0
Shutter, min. value [ $\mu\text{sec}$ ]	20
Shutter, max. value [ $\mu\text{sec}$ ]	24000
Pixel number	1248 x 1082

The SH-sensor is supplied with the software SHSWorks, enabling the customer to measure the wave front and compute different wave front specifications. In addition it provides the computation of the Zernike coefficients.

The SH-sensor software computes the Zernike coefficients out of the measured wave front. The coefficients state how pronounced each aberration type is in the wave front. Figure 3.2 shows a typical plot of the Zernike coefficients provided by the Optocraft software of a measured wave front.

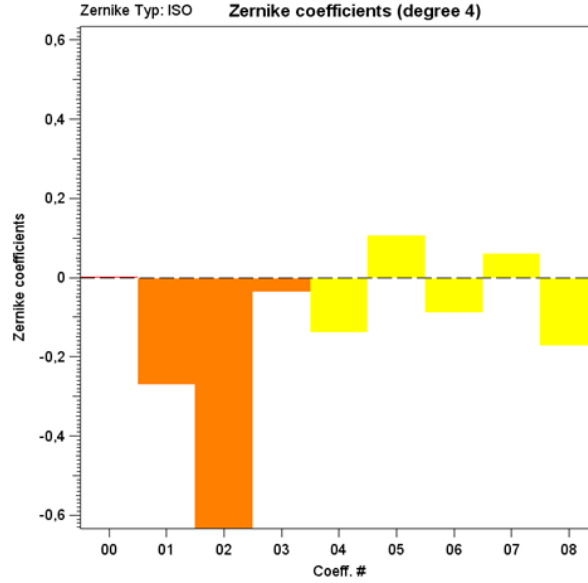


Figure 3.2: Typical plot of the Zernike coefficients (in  $\mu\text{m}$ ) during SH-alignment. 00...piston, 01...x-tilt, 02...y-tilt, 03...defocus, 04...astigmatism  $0^\circ$ , 05...astigmatism  $45^\circ$ , 06...coma x, 07...coma y, 08...spherical

As indicated in the manual the SH-sensor shows high thermal drift after turning it on. This must be taken into account when aligning the setup based on data measured with the SH-sensor. Especially for the collimator adjustment (as will be described later on) the thermal equilibrium must be reached before measurement. Figure 3.3 shows the change in the measured defocus coefficient due to thermal drift over a period of two hours. For this measurement a mirror was placed after the PBS and the light is back reflected without entering the telescopes. This was done to assure that there is no other drift source like e.g. the deformable mirror in the light path. The SH-sensor was turned off for 1 hour. In this time it cooled down. After that the SH-sensor was turned on again and logging of the Zernike coefficients was started.

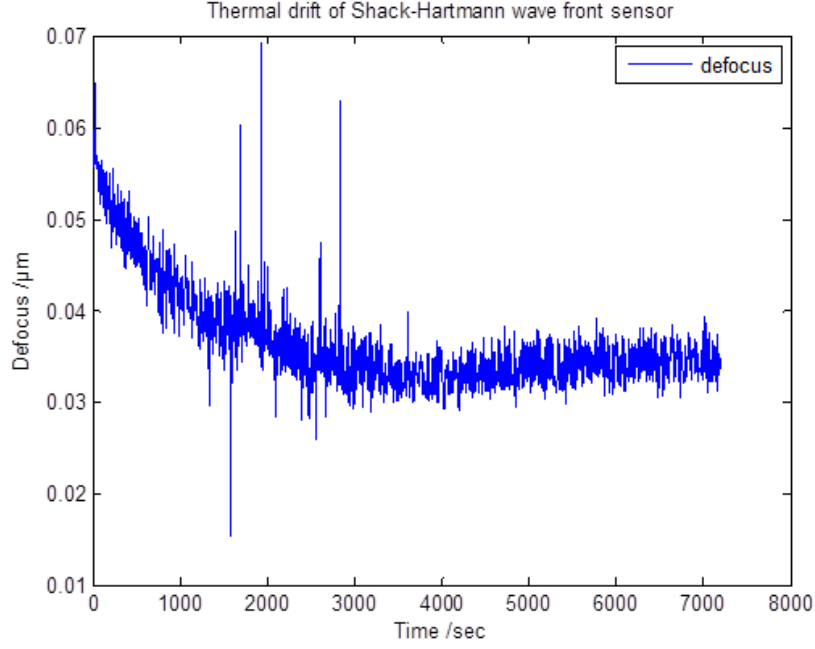


Figure 3.3: Thermal drift of the SH wave front sensor. Only the calculated defocus coefficient is shown.

### 3.1.3 Deformable mirror [23]

The deformable mirror (DM) Alpao HI-SPEED DM97-15 used in the setup consists of a membrane which can be deformed by 97 actuators. Since it is a mirror designed to correct high wave front aberrations it provides a large stroke. The deformable mirror is able to correct defocus and astigmatism up to  $45\text{ }\mu\text{m}$ . Further characteristics of the deformable mirror are shown in Tab. 3.3.

The actuator pattern is shown in Fig. 3.4.

The mirror can be driven with Matlab or LabVIEW. In this thesis the deformable mirror and the SH wave front sensor are driven with Matlab.

In order to test the stability of the DM the change in the defocus coefficient caused by a DM drift was investigated. For this purpose a mirror was placed at the location of the eye (c.f. Fig. 3.1) which back reflects the light. To make sure the SH-sensor stays in thermal equilibrium and the measured drift originates only from the DM the driving electronics of the DM was turned off, while the SH-sensor was turned on for 1 hour. Within two hours the measured defocus triples because of DM drift as shown in Fig. 3.5. For the closed loop mode the drift has no consequence but for alignment it must

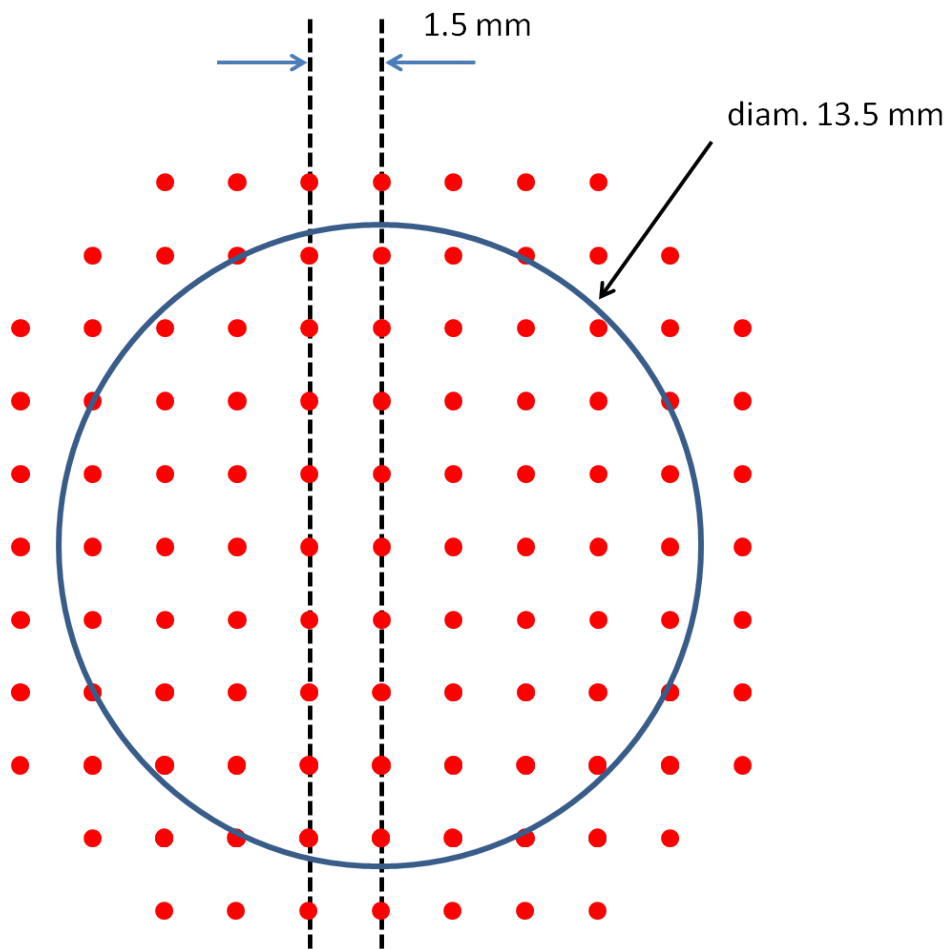


Figure 3.4: Actuator pattern of the DM adapted from [23]. The red dots are the actuators and the blue line is the clear aperture limit.

Table 3.3: Deformable mirror characteristics. [23]

Clear aperture size	13.5 mm
Number of actuators	97
Distance between two actuators	1.5 mm
Geometry of the actuators	Square grid
Mirror surface quality in closed loop	Error < 7.0 nm RMS
Wavefront tip/tilt stroke (Peak-to-Valley)	> +/- 60 $\mu\text{m}$
Wavefront astigmatism and focus (Peak-to-Valley)	> +/- 45 $\mu\text{m}$
Settling time (at +/- 5 %)	1 ms
Coating	Silver protected

be taken into account.

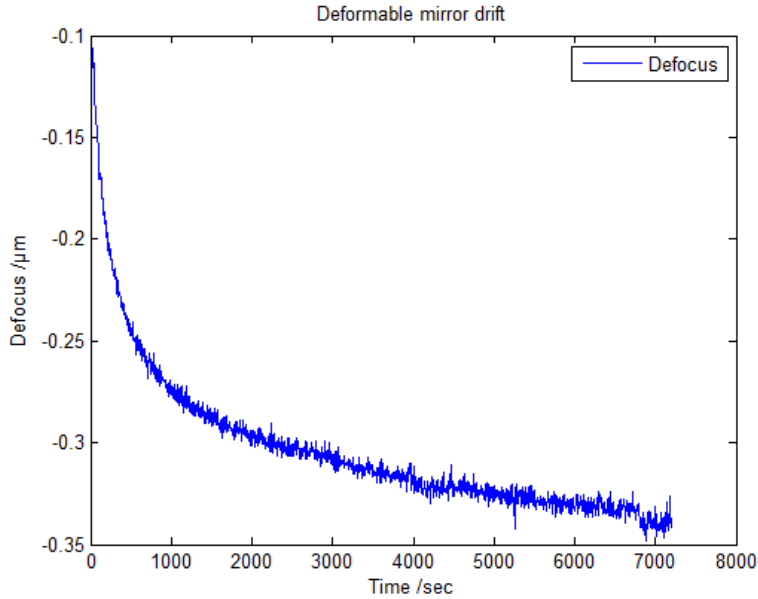


Figure 3.5: Measured drift over 2 h of the shape of the DM.

### 3.1.4 Resonant scanner [28]

The resonant scanner is responsible for line scans (x-direction). The scanner is a resonant scanner developed by the company GSI-Lumonics. It has a natural frequency of about 4 kHz. Further characteristics of the scanner and the scanner head are shown in Tab. 3.4. The use of a resonant scanner

is necessary to achieve great scanning speed as needed for line scans. The amplitude of the scanner head can be set manually with a potentiometer. The scanner provides a sync-signal which is used as master clock for a Field Programmable Gate Array (FPGA) unit which provides the driving signal for the Galvo scanner and the start trigger for the data acquisition.

Table 3.4: Resonant scanner characteristics. [28]

Natural frequency	3938 Hz
Frequency tolerance	+/-50 Hz
Maximum permissible angle	20°
Typical operating angle	15°
Mirror size	12.7 mm diameter
Useful aperture	12 mm x 9.25 mm
Surface accuracy	1/2 wave at 633 nm
Reflectivity at 45°	96 % above 600 nm

### 3.1.5 Galvo scanner [29]

The used Galvo scanner model 6230H is a moving magnet closed loop galvanometer based optical scanner from Cambridge Technology. The scanner is used to move the laser beam from one scanning line to the next. The driving signal is provided by the FPGA driving unit controlling both scanners. Some scanner characteristics are shown in Tab. 3.5.

Table 3.5: Galvo scanner characteristics. [29]

Rated angular excursion	40°
Maximum coil temperature	110°C
Small angle step response time	250 $\mu$ s, with 10 mm Y mirror, settled to 99 %

Whenever a line scan is finished by the resonant scanner, the Galvo scanner angle needs to be adapted to the next line. After the last line the scanner switches back to the first line. As a consequence the driving signal resembles a sawtooth signal as shown in Fig. 3.6.

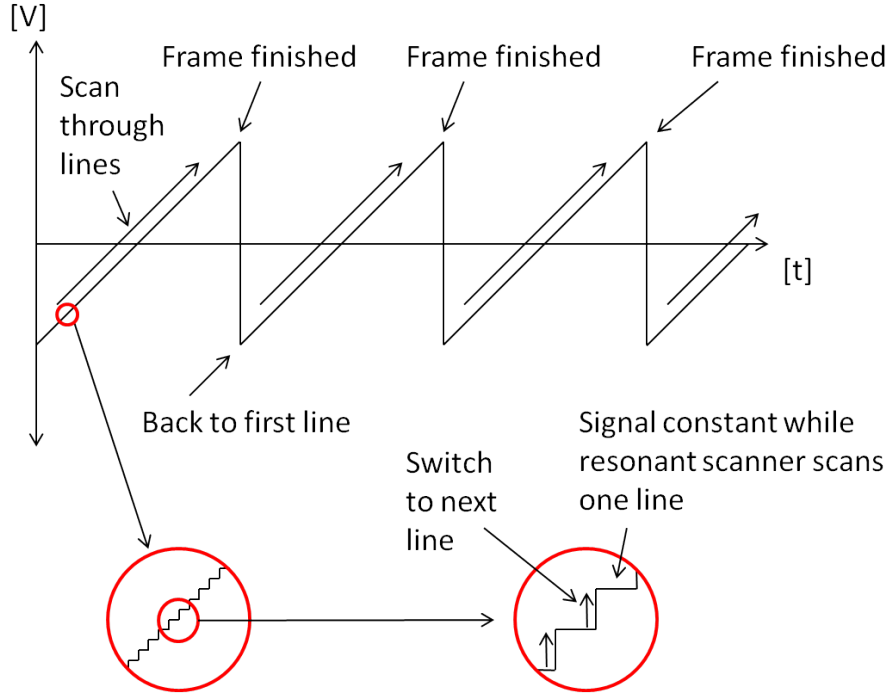


Figure 3.6: FPGA driving signal. The Galvo scanner moves the laser beam from one line to the next. Whenever a line is scanned by the resonant scanner the Galvo scanner adapts its angle to the next line. After the last line the scanning angle is set back to the first line.

### 3.1.6 Avalanche photo diode[30]

The avalanche photo diode (APD)-module used for the setup is the Si-APD-Modul LCSA500-10SMA from Laser Components. The characteristics of the APD are shown in Tab. 3.6.

### 3.1.7 Data acquisition board [31]

The data acquisition (DAQ) board used to measure the SLO data is the ATS9440 from Alazar Technologies. The main characteristics of the DAQ board are shown in Tab. 3.7.

### 3.1.8 Lenses

Table 3.8 shows the focal lengths of the lenses used in the setup shown in Fig. 3.1. All lenses used are coated for near-infrared applications.

Table 3.6: Characteristics of the APD-module. [30]

Wavelength range	400 nm - 1000 nm
Peak sensitivity	905 nm
Supply voltage	+12 V
Operating temperature	0°C - +50°C
Maximum incident light level (cw operation)	10 mW
Si-APD	SAR500
Active area diameter	0.5 mm
Bandwith	DC-10 MHz
Responsivity 540 nm	2.7 MV/W
Responsivity 650 nm	4 MV/W
Responsivity 905 nm	5 MV/W
Noise equivalent power 540	55 fW/rtHz
Noise equivalent power 650	37.5 fW/rtHz
Noise equivalent power 905	30 fW/rtHz
Output noise density	40 nV/rtHz

## 3.2 Beam propagation

### 3.2.1 Beam diameter

As described in the previous chapters in order to use the full aperture of the DM the beam diameter must be enlarged. After the DM, before the light enters the eye the beam diameter must be reduced. Table 3.9 shows the different beam diameter in the setup.

### 3.2.2 Light path

The light from the SLD enters the setup via the entrance collimator (c.f. Fig. 3.1). As the light is not entirely polarized it is necessary to polarize it with polarizer1. After that the light travels through a polarizing beam splitter (PBS) into the first telescope consisting of two achromatic lenses and an aperture. As mentioned before, polarization optics are used to avoid light from backreflections from the lens surfaces on the SH sensor. In the back focal plane of the second lens the y-scanner is placed. This scanner reflects the light into the second telescope which again consists of two achromatic lenses. The x-scanner is positioned at the back focal plane of the second telescope and reflects the light into the third telescope. At the back focal plane of the second lens of this telescope the deformable mirror is located.



Table 3.7: The main characteristics of the DAQ board ATS9440. [31]

Throughput	1.6 GB/s
Bus	PCIe x8
Channels	4
Real-time sampling rate	up to 125 MS/s
Resolution	14 bit
Input range	+/- 100 mW to +/-4 V
Bandwith	65 MHz
Memory per channel	up to 2 Giga-sample
Software development kit support	C/C++, C#, VB, MATLAB and LabVIEW

Table 3.8: Lenses used in the setup.

Lens	Focal length [mm]
L1	200
L2	200
L3	50
L4	50
L5	60
L6	100
L7	350
L8	180
Entrance collimator lens	40
Detector collimator lens	40

Via the DM the light enters the last telescope, traverses a quarter-wave plate oriented at  $45^\circ$  in respect to the incident polarization state. Therefore, the light is in a circular polarization state before it enters the eye. The human eye optics act like a collecting lens with the retina in its focal plane. As a consequence the collimated light is focused in a point on the retina (for an emmetropic eye). Depending on the tissue at that point more or less light is backscattered and exits the eye. This light traverses back through the quarter-wave plate, which changes the circularly polarization state to a linear polarization state (neglecting any birefringence effects of the eye), and all telescopes until it enters the PBS. The PBS now reflects the light from the sample arm in the detection arm because its polarization state has been rotated by  $90^\circ$  in respect to the incident light.

With this setup, light that is back reflected from any lens surfaces is greatly attenuated in the detection arm. Especially the wave front measure-

Table 3.9: Calculated beam diameter at different setup locations.

Location	Diameter [mm]
SH-sensor	8.0
Galvo scanner	8.0
Resonant scanner	8.0
DM	13.4
Eye	6.9

ment by the SH-sensor would be severely distorted by these back reflections.

Since the extinction ratio of the PBS is only 1:100 polarizer2 is implemented in the detection arm which suppresses the rest of the reflections with an extinction ratio of 1:100000. As a consequence the spot pattern is clear without disturbing spots arising from reflections on lens surfaces.

Figure 3.7 shows a typical SH-sensor image obtained from an artificial eye.

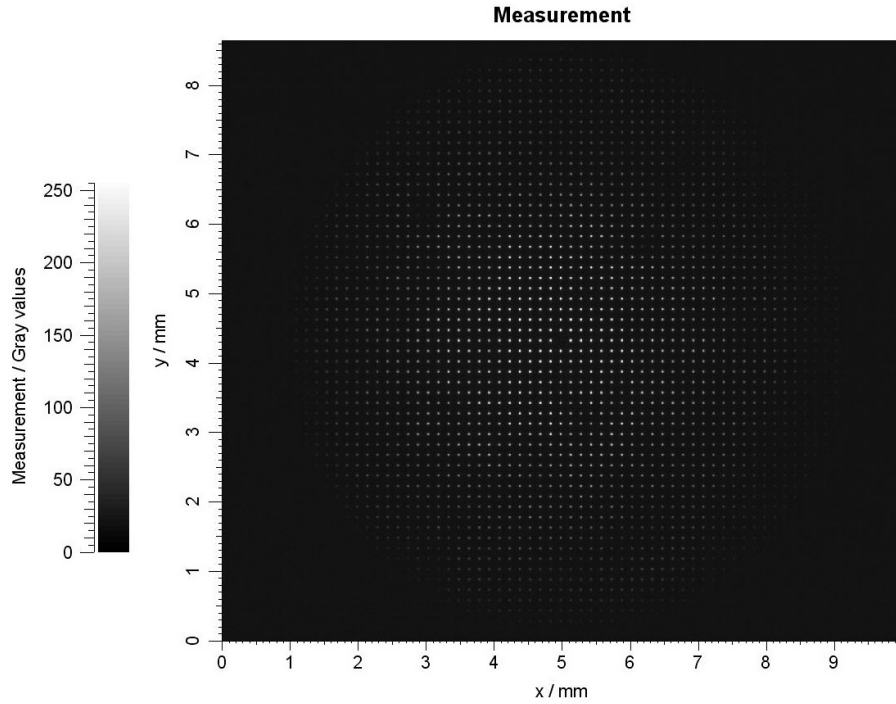


Figure 3.7: SH-sensor image of the artificial eye with quarter-wave plate in place. The two dimensional spot pattern is measured only from the artificial eye.

To demonstrate the effect of back reflections from the lens surfaces, the

quarter-wave plate was intentionally placed directly after the PBS (c.f. Fig. 3.1). After traversing the quarter-wave plate the light is in a circularly polarised state in all telescopes. Back reflections from lens surfaces traverse back through the quarter wave plate and will be in a linear polarized state oriented  $90^\circ$  to the incident state after traversing the quarter-wave plate a second time. The linear polarized light can pass through the PBS and polarizer2 and is measured on the SH-sensor. As a consequence the lens reflexes cause spots on the wave front sensor as shown in the outlined region in Fig 3.8. These undesired spots distort the spot find algorithm, the wave front measurement and finally the wave front correction.

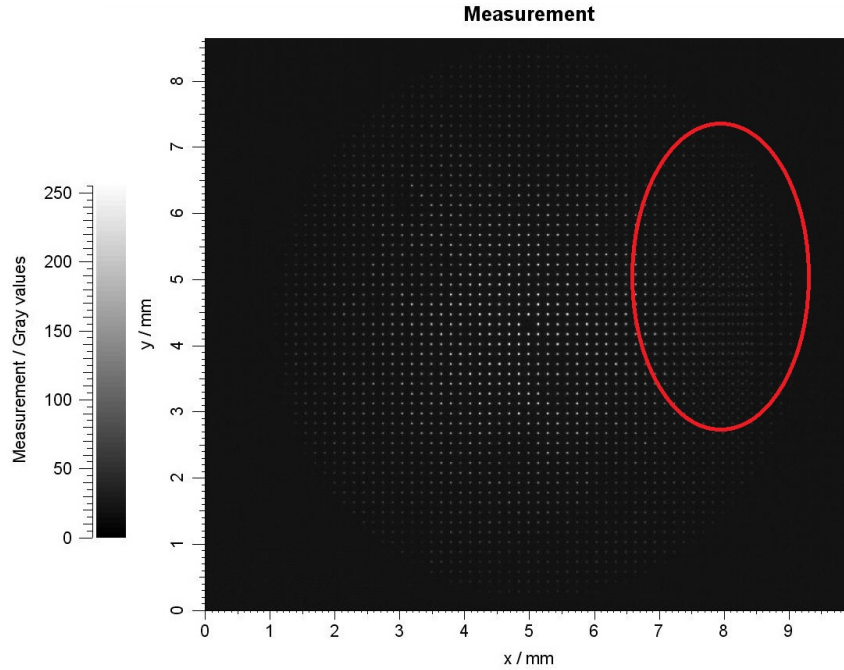


Figure 3.8: SH-sensor image with quarter-wave plate placed after PBS. In the outlined region undesired reflexes are visible.

After polarizer2 a pellicle is used to reflect 8 % of the light to the SH-sensor for the wave front measurement. The major part of the light is coupled into a single mode fiber (with a collimator) and is detected with an APD. The signal from the APD is recorded with a DAQ board.

# Chapter 4

## System alignment

This chapter deals with the alignment of an AO-SLO setup. As described in the previous chapters imaging of the wave front at the pupil plane of the eye onto the DM and onto the SH-sensor is essential for a good wave front correction. To achieve this each telescope between these components must be aligned perfectly. At first this chapter covers some prearrangements that have to be done before it can be started with building the actual setup. After that a detailed description of the AO-SLO alignment procedure will be given.

### 4.1 Prearrangements

#### 4.1.1 Collimator alignment

A collimator consists of a lens that is placed in a certain distance from the end tip of a single mode fiber. If the end tip is in the focal point of the collimator lens the light exits the collimator approximately as a plane wave. In order to test the collimation a setup was built consisting of the collimator and the SH wave front sensor (c.f. Fig. 4.1).

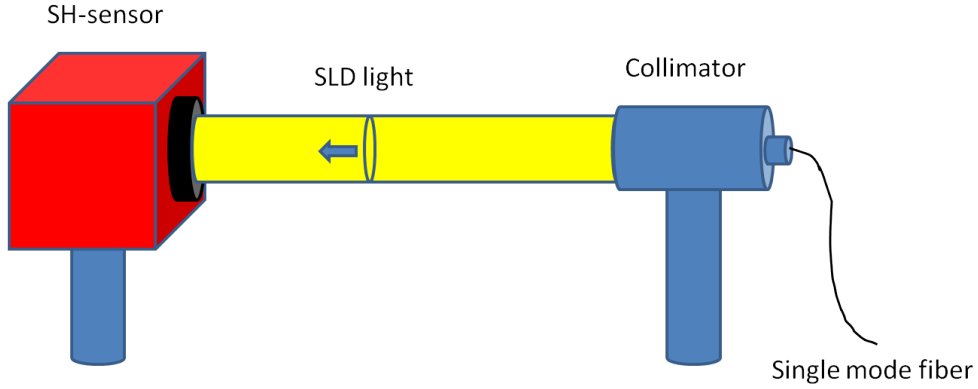


Figure 4.1: Setup for testing the collimation of the collimator

The collimators used in the setup are custom designed to enable a precise alignment of the lens position. This is necessary because the collimation using commercially available products is not accurate enough. Each collimator consists of two cylinders that can be telescoped. One cylinder holds the lens, while the other holds the end tip of the single mode (SM)-fiber. Therefore the distance between SM-fiber and lens can be adjusted. To find the exact focal distance, light from the SLD was coupled into the SM-fiber. The SH-sensor was positioned opposite to the collimator and was used to measure the wave front, especially the defocus coefficient.

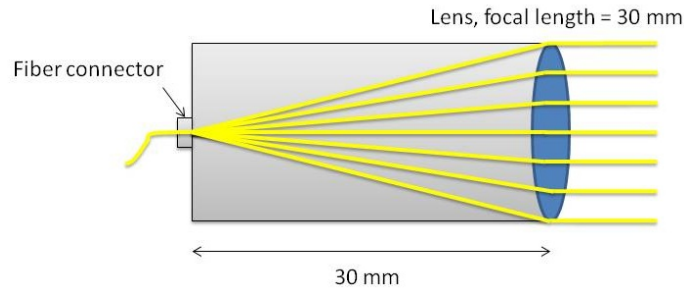


Figure 4.2: Beam geometry in the case of a well adjusted collimator.

The exact alignment is difficult to achieve because a small change in the distance results in a relative high change of the defocus coefficient. When according to the SH-measurement the right position is found (c.f. Fig. 4.2), cross-checks should be made. There are two ways: 1. To look at the light beam over a long distance with an IR-sensor card. The size of the light beam should stay constant over the distance. 2. The more accurate cross-check is

to couple the light exiting from one collimator into a SM-fiber connected to another after adjusting both.

In the case of good alignment it should be possible to couple 2/3 of the light power from one SM-fiber into the other. If one of the cross-checks doesn't work as expected the collimators must be adjusted again.

### 4.1.2 Determination of the setup height

Most optical elements like lenses or the aperture are mounted on posts. These posts can be fixed into post holders and those can be attached to the optical table via clamps as shown in Fig. 4.3. Since the height of a lens can simply be increased or decreased by sliding the post out of the post holder or sliding it into the post holder these elements don't determine a special height.

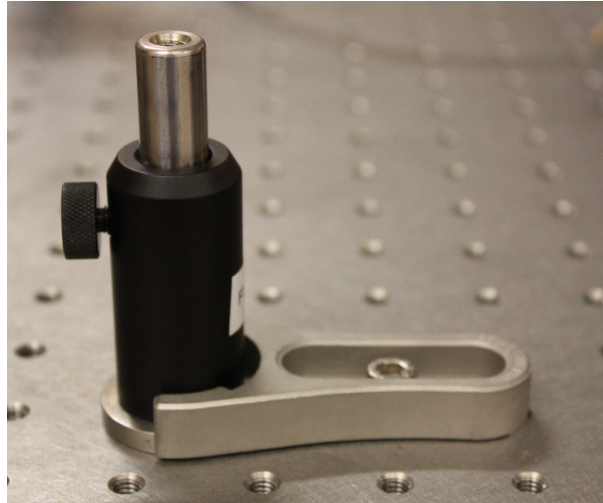


Figure 4.3: Post holder with post mounted on the table with a clamp.

For some devices mountings had to be fabricated, for instance the DM. Since the mounting of the DM is not designed to be changeable in height, the DM determines the system height. The optical axis of the system was adjusted to this fixed height (center of the DM).

## 4.2 Adjusting the entrance collimator

Adjusting the entrance collimator is a very crucial part and should be done as accurate as possible. The collimator is fixed in a mounting allowing the collimator to be tipped and tilted. The light exiting the collimator should

be parallel to the optical table and at the height of the DM. Otherwise astigmatism in the first telescope will be introduced. To check this condition the height of the light beam is measured at different distances from the collimator.

### 4.3 Alignment of SH-sensor to entrance collimator

Since the SLO setup is enhanced with AO, accuracy is very important. Imaging the deformable mirror onto the SH wave front sensor by the lens system is crucial, otherwise AO would not work properly and the improvements of the system in comparison to a SLO without AO would be distorted. As can be seen in Fig. 3.1 after the collimator a Thompson polarizer has to be placed. This polarizer must be positioned correctly to avoid cutting off the laser beam. The best way to accomplish this is to observe the beam on a fixed mounted infra-red sensor card when introducing the polarizer. The position of the beam on the card shouldn't change when the polarizer is placed in or out. The polarizer is followed by a polarizing beam splitter. Similar to the polarizer the PBS needs to be adjusted in position and height to avoid cutting off the laser beam. After implementing the collimator, the polarizer and the PBS the height and the angle of the beam should be checked again by measuring the height at different distances from the PBS. It can be necessary to slightly adjust the tilt of the entrance collimator since the polarizer and the PBS may change it. Now again a cross check if the beam position remains in the same height over a distance of two meters must be performed. If the setup passes this test the parts mustn't be changed any more.

In a next step a mirror is positioned after the PBS to reflect the light back to the collimator (c.f. Fig. 4.4). This mirror is aligned (tilt by x and y) until as much light as possible is coupled back into the SM-fiber. In order to direct the light into the measurement arm of the setup a quarter-wave plate oriented at  $45^\circ$  to the incident polarization state has to be placed between the PBS and the mirror.

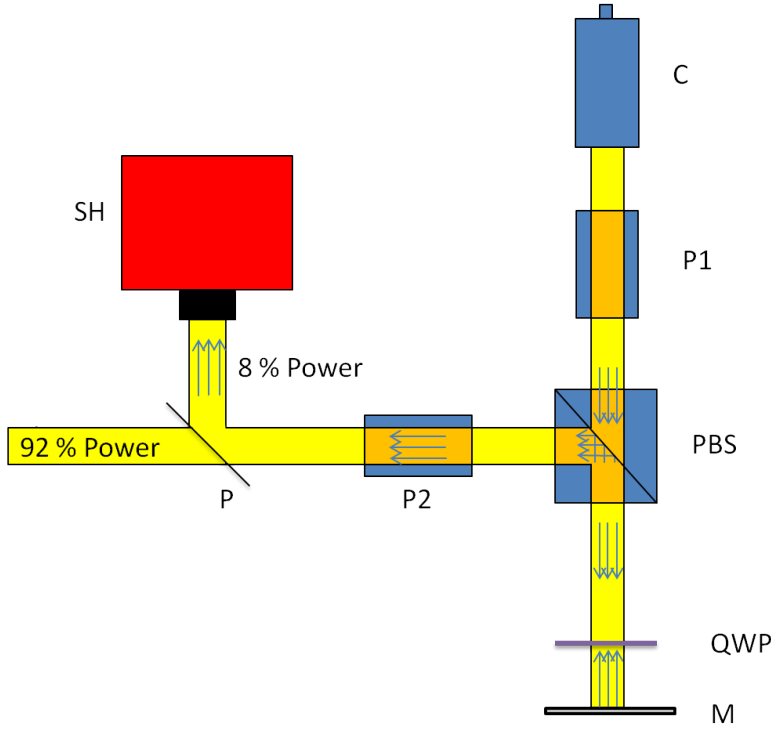


Figure 4.4: Setup for aligning the SH-sensor. C...Collimator, P1...polarizer 1, PBS...polarizing beam splitter, P2...polarizer 2, P...pellicle, QWP...quarter-wave plate, SH...SH wave front sensor, M...mirror

It must be ensured that the PBS reflects the light parallel to the table and normal to the incident light beam. Similar as the collimator tilt this can be checked by measuring the beam height with an IR sensor card at different distances from the PBS. Now a pellicle beam splitter has to be added to the optical path to divert 8 % of the light power for measurement on the SH-sensor. The transmitted light will be used for imaging. The pellicle should be placed at an angle of about  $45^\circ$  to the propagation direction of the light beam. The alignment of the SH-sensor is performed using the data from the SH-sensor itself. For height and x-alignment the direct SH-signal (spot diagram) is used. The position is changed until the light beam is central on the sensor with the maximum of the Gaussian beam profile centred at the middle of the sensor chip. After that the evaluation software can be used to compute the Zernike coefficients of the wave front in order to determine the tilt of the wave front. Fig. 3.2 shows a typical plot of the Zernike coefficients.

To correct the x-tilt the SH-sensor must simply be rotated along the vertical axis. The y-tilt can be corrected with a goniometer on which the SH-sensor is mounted. Very small rotation results in a huge change in the Zernike



coefficient and it might take some time to find the best alignment. However the coefficients should be smaller than  $0.1\mu\text{m}$  (beam diameter: 8 mm). This alignment procedure is very accurate and can be repeated even in case of unintentional misalignment of the SH-sensor in a later stage of the alignment procedure.

## 4.4 Alignment of first lens to SH-sensor

Since the SLO is enhanced with AO it is crucial that the plane of the deformable mirror is imaged onto the SH-sensor. As a consequence the wave front sensor has to be located in the back focal plane of the first lens.

Because the wave front in an AO-system is optimized at the location of the SH-sensor (and therefore at all imaging planes that are conjugate to the SH-sensor), the collimator for coupling the light into a SM-fiber for imaging should be placed at the same imaging plane. In some applications (e.g. polarization sensitive imaging) the light which is back-coupled into the entrance SM-fiber is used. Therefore the entrance collimator should as well be placed at this imaging plane. Note that simply placing the lens at the focal distance to the collimator is too inaccurate.

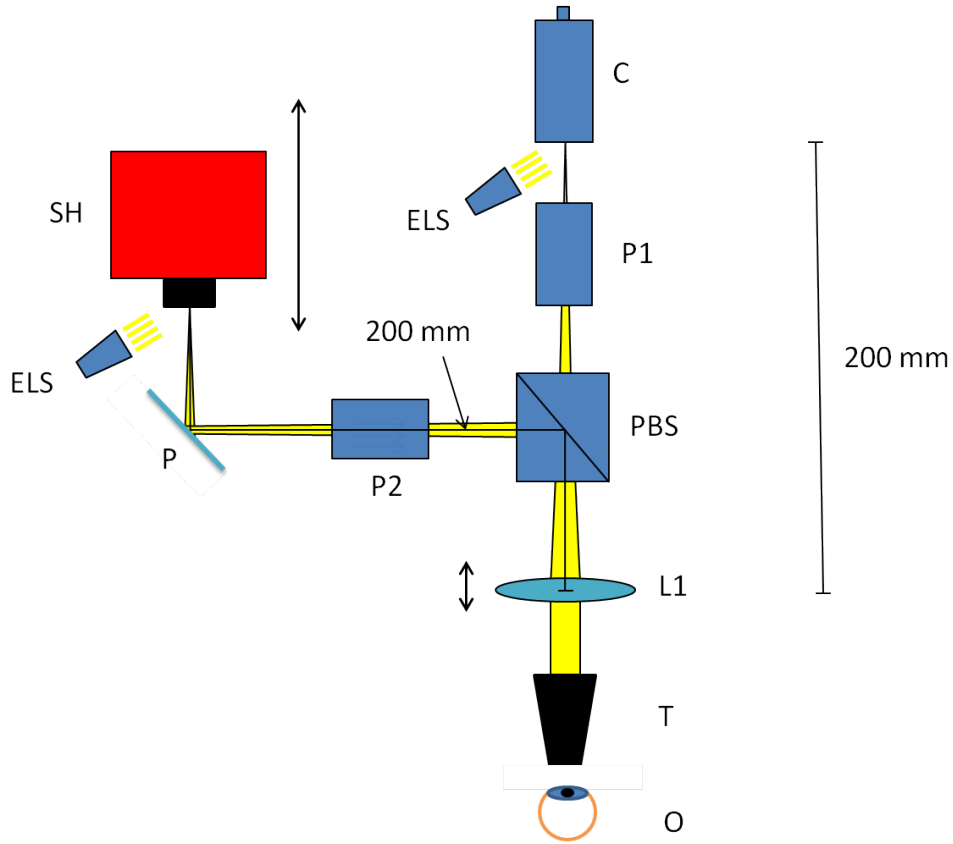


Figure 4.5: Setup for the alignment of the first lens and the axial position of the SH-sensor. SH...SH wave front sensor, ELS...external light source, C...collimator, P1...polarizer 1, PBS...polarizing beam splitter, P2...polarizer 2, L1...first lens, T...telescope, O...observer, P...pellicle

To find the right distance between the entrance collimator and the first lens a common telescope is used. First the telescope has to be adjusted for infinity. One can use the moon or a very far object. That object must be peered at and the telescope must be adjusted until the image appears sharp. It is inevitable to use the same eye for adjusting the telescope and the lens since the two eyes of one person are never exactly the same, which would add additional alignment errors. Now that the telescope is adjusted it can be used to look towards the lens while highlighting the entrance collimator with a flash light as shown in Fig. 4.5. It is crucial to turn off the laser before looking into the telescope, otherwise the retina can be damaged. If the distance between the collimator and the lens commensurates to the focal length of the lens, dust on the collimator lens' surface can be seen. By shifting the lens forward and backward the right distance, where the collimator lens'

surface is seen sharp, can be found. When shifting the lens forward and backward the x-position of the lens may be changed. So after the right position with a sharp image is found, an infrared sensor card is used to check if the beam is still central on the lens. Usually these steps have to be repeated until the image is sharp and the beam is centered on the lens.

In a next step the distance between SH-sensor and first lens has to be aligned. Since the lens has been fixed in the previous step, the sensor position must be changed. Similar to the previous alignment step the SH-sensor is illuminated with the flashlight and the telescope is used as shown in Fig. 4.5. The wave front sensor has to be moved forward or backward until the lenslet array can be seen sharp. After the right position is found the sensor must be fixed and not be changed any more.

Now the first part of the setup is aligned. However, even if worked very accurate there will be a small inevitable error in the position of SH-sensor and first lens due to chromatic aberration. Chromatic aberration results in different focal lengths for different wavelengths. Since the visible light spectrum was used to find the right position but the setup will later be used for 840 nm light a residual small error in the position remains.

It is very important to avoid even the slightest changes in any of the included parts. One special risk for misalignment are the cables of the SH-sensor. They can accidentally be touched during alignment of the rest of the system. However in this case it is possible to find the exact sensor position again by introducing a mirror into the setup that couples the light into the entrance SM-fiber and centering the beam on the sensor.

## 4.5 Alignment of first telescope and aperture

As can be seen from Fig. 4.6 The first telescope contains two 200 mm lenses located between the PBS and the Galvo scanner. In the first telescope an aperture is inserted in order to further suppress back reflections from the lenses. In addition the aperture helps for aligning all four telescopes of the system. Two reference points are used for the alignment. First, the beam position on the SH-sensor (which can be determined very accurate) and second, the aperture. This ensures that the beam propagates only along the optical axis of the system.

The aperture should be aligned precisely because an error in its position will affect the alignment of all telescopes. At first an aligned mirror is placed in front of the Galvo scanner together with the quarter-wave plate and adjusted that the back reflected beam is centered on the wave front sensor. The quarter-wave plate has to be placed in a part of the setup in which the light is

collimated. Otherwise the quarter-wave plate, acting as a plan parallel plate would change the measured wave front, especially the defocus coefficient.

Since the first lens has already been aligned one can proceed with the second lens. First the lens is placed roughly at the desired position (a simple tape measure can be used) and the x-y position is checked using an IR-sensor card. The beam should be at the center of the lens. For fine adjustment the wave front sensor is used. The software computes the Zernike coefficients of the wave front and displays them in a Zernike bar plot. With this help the x- and y-tilts of the wave front caused by misplacement of the lens can be minimized. After minimizing it the defocus can be reduced by shifting the lens forward and backward relative to the light propagation direction. Since the Zernike coefficient measurement is very sensitive, little changes in the lens position cause huge changes of the Zernike coefficients. As a consequence the shifting of the lens forward and backward will always introduce little tilts. However, the Zernike coefficients have to be iteratively reduced until tilts are at least smaller than  $0.1\text{ }\mu\text{m}$  and defocus is equal to or smaller than  $0.01\text{ }\mu\text{m}$  at a beam diameter of 8 mm.

In a next step the aperture must be added. Similar to the second lens it can be placed roughly between the two lenses using a tape measure. At this stage the aperture is completely open. By reducing the size of the aperture the beam will be cut off at some point, if the aperture is not at the correct position. In this case it must be shifted relative or perpendicular to the light propagation direction or raised or lowered until no cutting off can be observed. If it is not possible to set the aperture to the smallest diameter ( $\sim 0.75\text{ mm}$ ) without cutting off the beam the first telescope must be realigned.

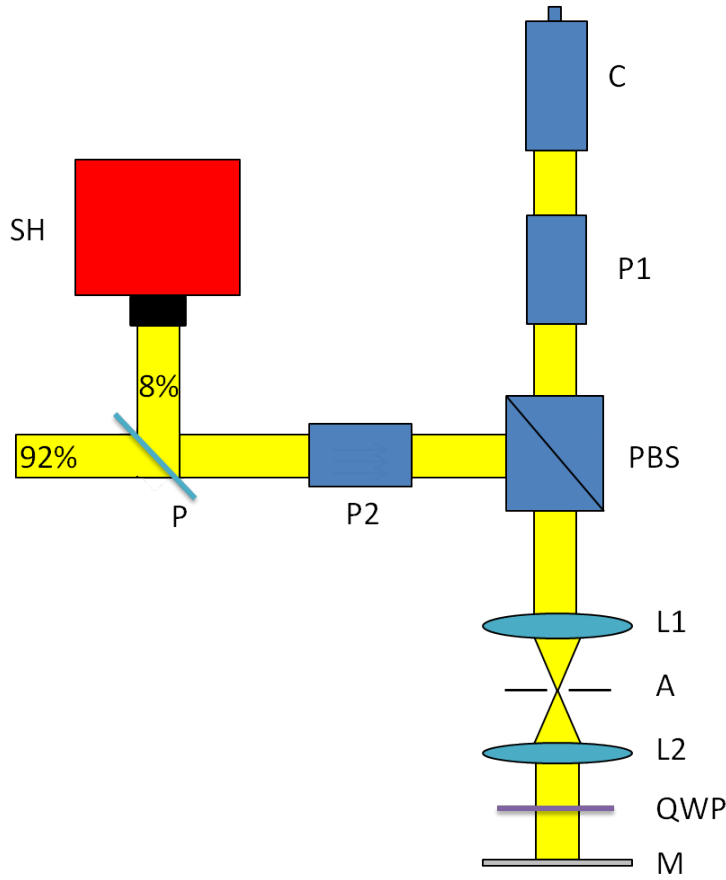


Figure 4.6: Setup for aligning the first telescope. C...Collimator, P1...polarizer 1, PBS...polarizing beam splitter, P2...polarizer 2, P...pellicle, QWP...quarter-wave plate, SH...SH wave front sensor, L1...lens 1, L2...lens 2, M...mirror

## 4.6 Alignment of the Galvo scanner

The Galvo scanner is responsible for the up and down scan. The mirror used to align the first telescope in the previous section must now be replaced by the Galvo scanner. The Galvo scanner must be placed in the back focal plane of the second lens of this telescope and aligned in order to back reflect the light similar as the alignment mirror did. Further the Galvo scanner must be hit by the beam at the center to avoid cutting of the beam.

For alignment it is essential to connect the scanner to its driving unit and turn the power on. If not done so, the scanner head angle will be random and reasonable alignment is not possible. With the driving electronics the

angle should be set to a distinct value, optimally in the middle of the scanner's range of rotation. With a measuring tape the scanner is placed approximately at a distance of 200 mm from the second lens. This can be checked with an infra-red sensor card. If the beam doesn't hit the Galvo scanner at the center of its mirror head it must be adapted by changing height and position perpendicular to the light propagation direction of the Galvo scanner. After aligning the scanner position tip and tilt of the scanner are changed until the beam can be observed with the wave front sensor. To simplify finding the right tip and tilt of the scanner the aperture should be opened. Note that the aperture rejects light paths that are not co-axial to the optical axis. The smaller the aperture the more accurate the light path is restricted to the optical axis. For a rough alignment an infra-red sensor card with a little hole can be used. The hole allows the incoming light to pass the card and to watch the reflected light on the sensor card. Now the scanner can be tilted until the reflected light traverses back through the hole. After that the beam can be observed on the wave front sensor or at least after a small change in the tilt of the Galvo scanner. At next the beam should be centered as well as possible. Then the aperture size can be reduced until the beam is cut off. By slightly adjusting the Galvo scanner tilt the cutting off can be avoided. After that the size of the aperture can be reduced again until it cuts off the beam and again the Galvo scanner tilts must be changed. After some repetitions of these steps the aperture should be set to the minimum diameter and the beam shouldn't be cut off and is centered on the wave front sensor.

Now the Galvo scanner is adjusted to reflect the light beam into itself but the position along the optical axis is not yet aligned. The scanner has to be placed in the focal plane of the second lens. To find the correct position the following procedure can be used: To start with, the first lens has to be removed from the setup and the aperture has to be opened. As a consequence the light is still collimated until it reaches the second lens. Since the light between second lens and Galvo scanner is not collimated any more, the quarter-wave plate must be put at a different position (i.e. before the second lens). Now the wave front sensor can be used to find the correct position of the scanner. The measured defocus coefficient will only be zero when the scanner is placed exactly in the focal plane of the second lens.

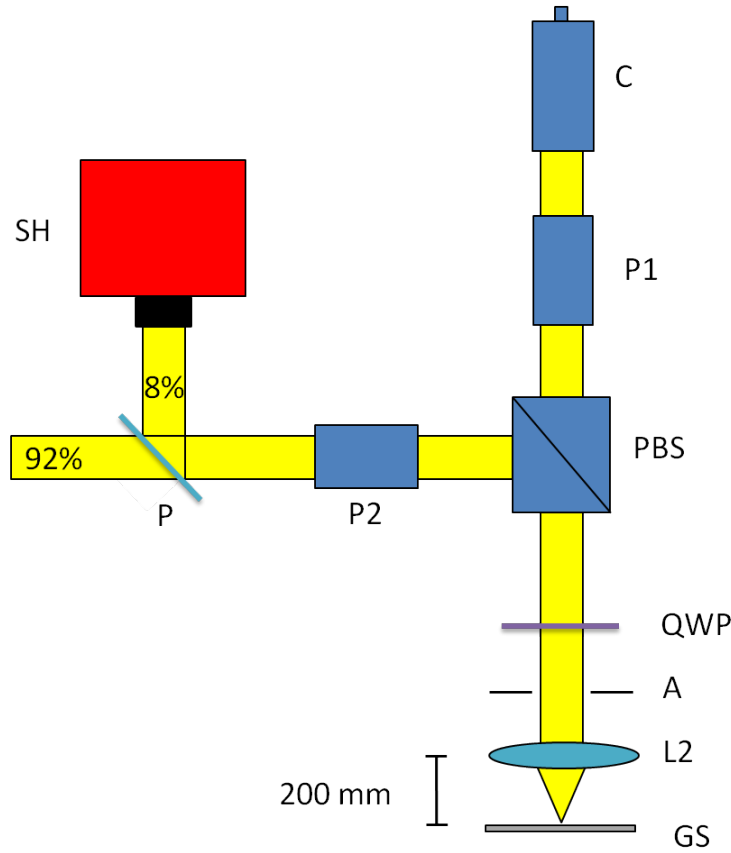


Figure 4.7: Setup for finding the correct position of the Galvo scanner. C...Collimator, P1...polarizer 1, PBS...polarizing beam splitter, P2...polarizer 2, P...pellicle, QWP...quarter-wave plate, SH...SH wave front sensor, A...aperture, L2...lens 2, GS...Galvo scanner

To achieve this the Galvo scanner has to be moved forward and backward relative to the light propagation direction without tilting it or shifting it perpendicular to that direction. Hereby it is best to use the Zernike bar plot and keep an eye on tip and tilt while trying to set the defocus coefficient to zero. When the defocus coefficient is close to zero the central position of the light beam on the mirror has to be checked. After this step the first lens can be put in again and the aperture can be set to the minimum diameter. If the beam is cut off, the first lens will be removed again and the scanner will be adapted like before. It is usual to repeat these steps many times until satisfying results are obtained.

The correct position is found and the first telescope is finished, when the defocus is smaller than or equal to  $0.01\mu\text{m}$  (beam diameter: 8 mm) and the beam is not cut off by the aperture while remaining at the center of the

SH-sensor.

## 4.7 Alignment of the second telescope

The principle of the second telescope is similar to the first telescope. This time the wave front needs to be imaged from the Galvo to the resonant scanner. Difficulties arise from the short focal length of the used lenses. Both lenses have a focal length of 50 mm, determining the length between the scanners to  $\sim 200$  mm. The short focal distance makes the alignment even more difficult than the alignment of the first telescope, since small errors in the position now create even larger wave front aberrations than in the first telescope (containing two 200 mm lenses).

At first the Galvo scanner needs to be rotated around the vertical axis to reflect the light into the direction of the second telescope as shown in Fig. 4.8. As cross check the angle of the light beam needs to be controlled by measuring the signal height at different distances from the Galvo scanner. In the case the light doesn't travel parallel to the optical table its direction has to be corrected by rotating the Galvo scanner along the horizontal axis (the mounting of the Galvo scanner allows a smooth rotation around this axis). Now an alignment mirror must be placed at a distance of about 300 mm from the Galvo scanner. As before the tilt of the mirror is adjusted using the infra-red sensor card. After that with little change in the mirror's tip and tilt the beam should already be observable with the SH-sensor. Then, by stepwise reducing the aperture size and recentering the beam on the SH-sensor, after some repetitions, the beam shouldn't be cut off any more when the aperture is set to the minimum diameter.

The next element is the first lens of the second telescope. This has to be positioned at the focal distance from the Galvo scanner. To make sure that the lens does not change the direction of light propagation the beam location should be watched on a fixed mounted infra-red sensor card before the mirror when putting in the lens. The beam remains at the same position when the lens plane is perpendicular to the incident light propagation direction. Now the first lens of the first telescope must be removed and the position of the first lens of the second telescope is aligned using the Zernike bar plot of the SH-sensor. Like in the first telescope it is inevitable to shift the lens perpendicular to the light propagation direction. By shifting the lens the Zernike coefficients have to be iteratively reduced until the tilts are smaller than  $0.1 \mu\text{m}$  and the defocus is smaller than  $0.01 \mu\text{m}$  (beam diameter: 8 mm).



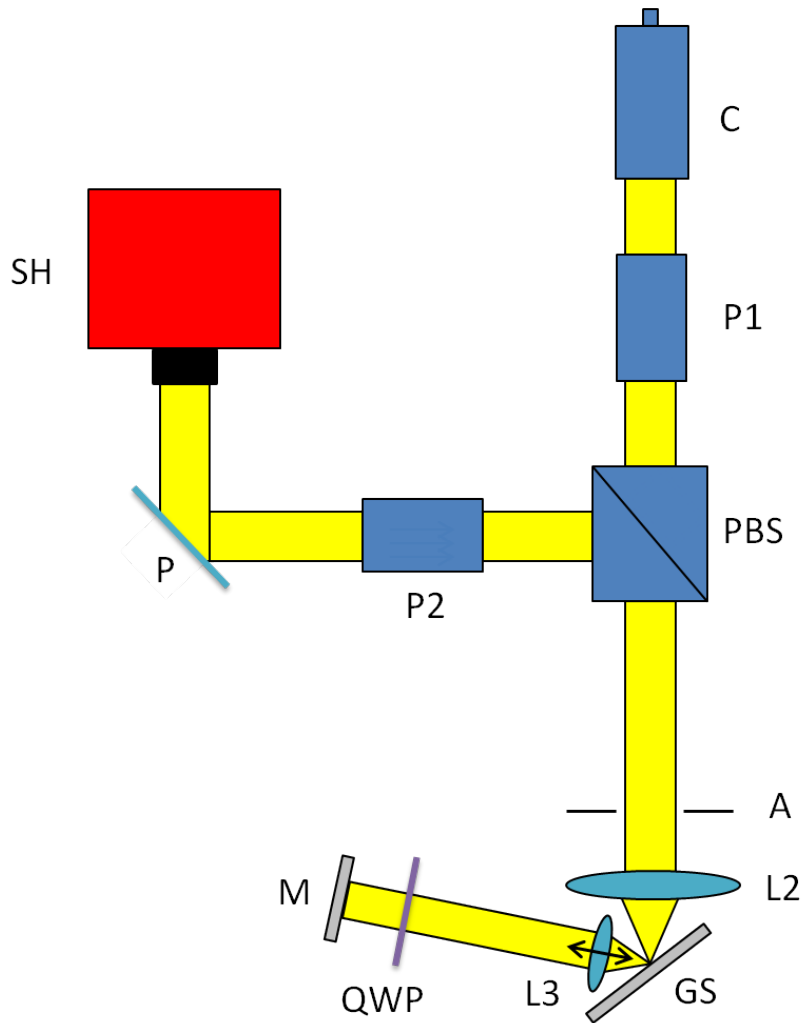


Figure 4.8: Setup for aligning the first lens of the second telescope. C...Collimator, P1...polarizer 1, PBS...polarizing beam splitter, P2...polarizer 2, P...pellicle, QWP...quarter-wave plate, SH...SH wave front sensor, A...aperture, L2...lens 2, GS...Galvo scanner, M...mirror

In order to align the second lens of the second telescope, the first lens of the first telescope must be installed again.

Again the correct position is found by shifting the lens until the measured defocus is close to zero. After the alignment the position of the beam on the wave front sensor and the beam cutting off must be checked.

In a next step the resonant scanner has to be aligned. Therefore the alignment mirror must be removed and replaced with the resonant scanner. At first the resonant scanner is roughly positioned in the focal plane of the

second lens of this telescope. Similar to the procedure with the Galvo scanner, the tip and tilts of the resonant scanner have to be aligned. The distance between resonant scanner and second lens of the second telescope has to be found. To do so the first lens of the first telescope has to be removed. Then the resonant scanner is shifted until a minimum of defocus is measured with the SH-sensor. Thereby it is mandatory to keep an eye on the tilts, too. The alignment is acceptable if the defocus is below  $0.01\text{ }\mu\text{m}$  (beam diameter: 8 mm). Then the first lens of the first telescope must be installed again and the position of the beam on the wave front sensor and the eventual cutting off must be checked. In the case of a failing of the check the scanner position must be changed and the procedure is repeated until the telescope passes these tests.

## 4.8 Alignment of the third telescope and the deformable mirror

The third telescope consists of lenses with different focal lengths. The first lens has a focal length of 60 mm and the second lens has a focal length of 100 mm. Therefore, the diameter of the light beam is enlarged. This ensures the whole diameter of the DM is illuminated.

At first the light must be reflected from the resonant scanner to the telescope. This can easily be done by turning the resonant scanner until the desired direction is reached. Now at different distances from the resonant scanner the height of the light beam needs to be checked and adjusted to ensure a propagation that is parallel to the table. After that the alignment mirror is placed at the end of the telescope and aligned for reflection (i.e. beam is centered on the wave front sensor). Now the lenses of the third telescope are aligned analogue to the previous telescopes.

The measured defocus after the third telescope should be equal to or smaller than  $0.01\text{ }\mu\text{m}$  (beam diameter: 8 mm). When done properly the beam is centered on the wave front sensor and is not cut off by the aperture. When the telescope passes these cross checks the DM can be aligned. Otherwise the previous steps need to be repeated.

Now the alignment mirror at the end of the telescope needs to be replaced by the DM. The reflecting membrane of the DM has to be placed in the focal plane of the second lens. The same techniques as before can be used. However, it is important to flatten the mirror before adjusting the position. When flattening the DM the drift has to be taken into consideration. To avoid misalignment of the DM because of its drift the DM must be flattened

only for one minute and then reset again whenever it is used for aligning. The first lens of the first telescope has to be removed and the DM has to be shifted until the defocus is equal to or smaller than  $0.01\text{ }\mu\text{m}$  (beam diameter:  $8\text{ mm}$ ) (c.f. Fig. 4.9).

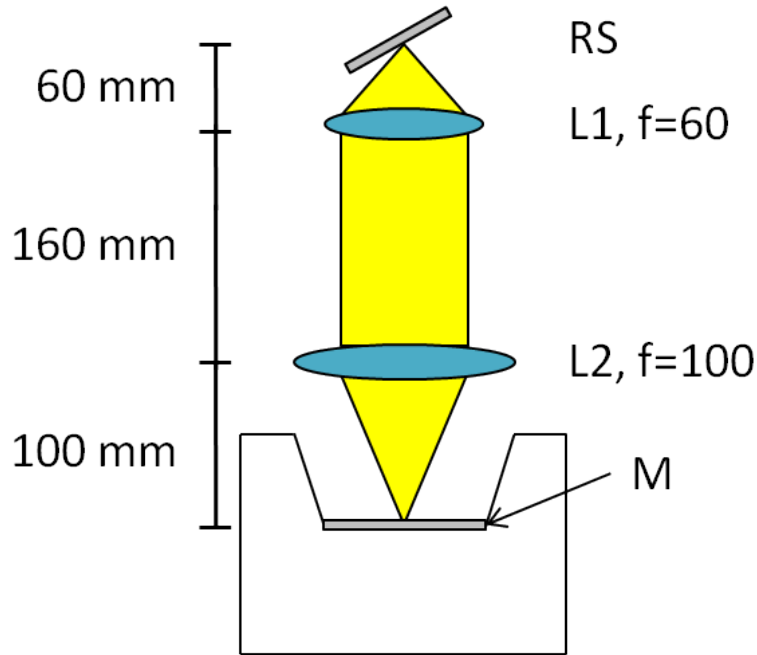


Figure 4.9: Correct position of DM during alignment. L1, L2...lenses, DM...deformable mirror, RS...resonant scanner, M...membran of deformable mirror. Note that the first lens of the first telescope is removed during this procedure.

Although only the focal spot of the light beam is reflected a non plane membrane will cause an error in the alignment. After the correct position is found the first lens of the first telescope is put into the setup again and cutting off the beam with the aperture needs to be checked.

The status of the third telescope and the DM is shown in Fig. 4.10.

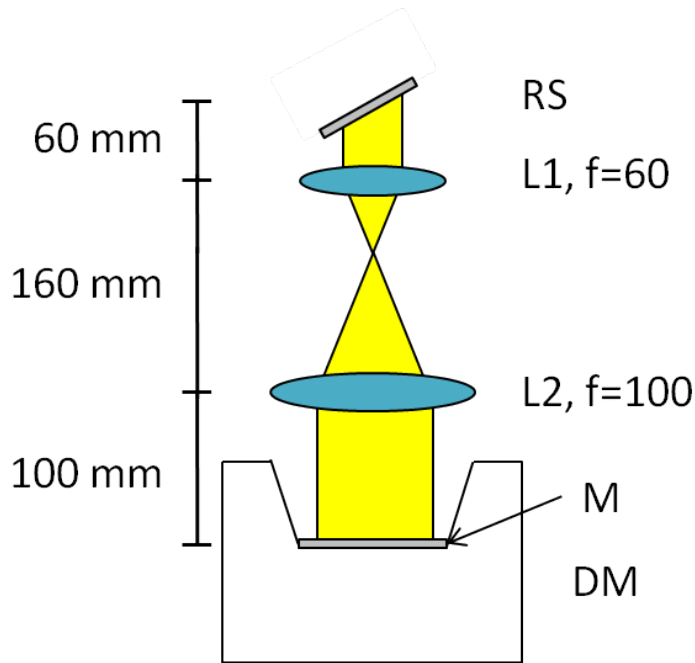


Figure 4.10: Status of the third telescope after alignment. L1, L2...lenses, DM...deformable mirror, RS...resonant scanner, M...membran of deformable mirror.

Now all telescopes between entrance collimator, SH-sensor and DM are aligned. At this point the adaptive optics loop can be tested in order to check the quality of the alignment. In case of good alignment (i.e. the plane of the DM is imaged onto the SH-sensor) the AO loop should reduce the wave front's RMS and should run stable, without over driving the actuators of the DM.

Figure 4.11 shows a successful example of a stable running closed loop. At the point at which the loop is closed the RMS of the wave front decreases from  $0.6\text{ }\mu\text{m}$  to about  $0.03\text{ }\mu\text{m}$ . The DM's actuators can be seen in the calculated wave front, which indicates a well aligned setup. Figure 4.12 shows each actuator and its current driving signal between -1, maximum pull, and 1, maximum push. It also shows the latest maximum command. If this value stays in a small interval the AO closed loop runs stable.

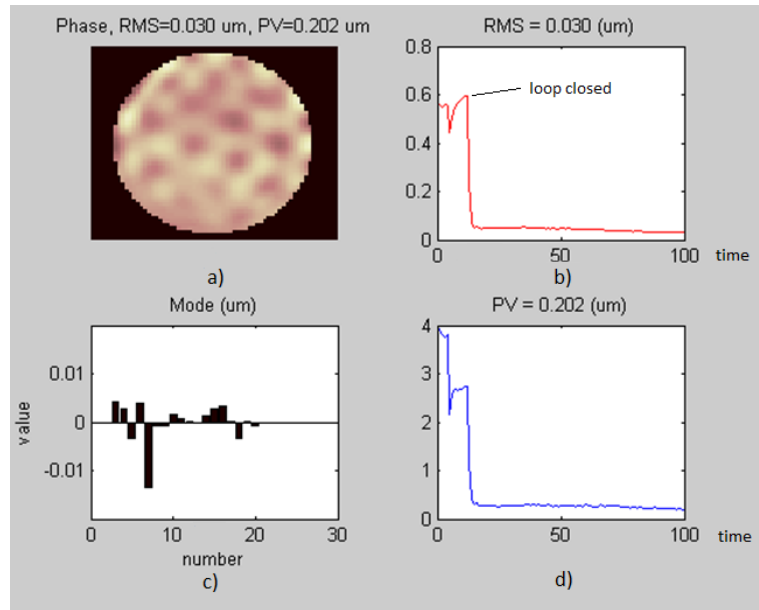


Figure 4.11: Example of a stable running AO-loop. a) current waveform, b) RMS error of the wave front, c) current Zernike bar plot, d) maximum peak to valley (PV) of the wave front. Tip and tilt are excluded from the calculation.

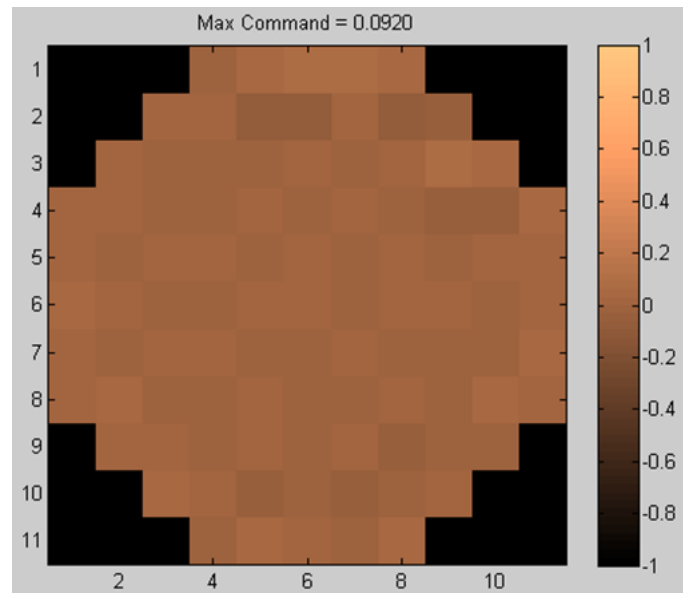


Figure 4.12: Mirror monitor showing the driving signal of each actuator of the DM between -1...maximum pull and 1...maximum push

## 4.9 Alignment of the fourth telescope and the Badal system [32]

The fourth telescope consists of one lens with a focal length of 350 mm and another one with a focal length of 180 mm. Since they are arranged in this order they reduce the beam diameter. The beam is reflected over a Badal system [32], allowing to change the distance between the two lenses. This can be used to correct defocus originating from a patients' ametropia. Correcting the constant defocus of the human eye at this point saves driving range of the DM for higher order correction (c.f. Fig. 4.13).

At first the DM needs to be flattened (as mentioned before always only for short times because of its drift) and turned, so that the light beam is reflected to the fourth telescope. At different distances from the DM the height of the light beam has to be checked. Before aligning the lenses the Badal system is implemented. It consists of three gold-coated prism mirrors. Two prism mirrors are mounted on a translation stage which enables a change of the distance.

The alignment of the fourth telescope is done identical to the previous telescopes.

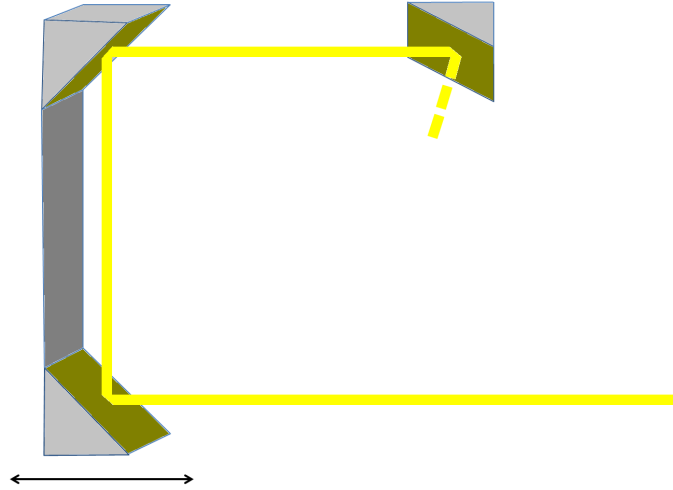


Figure 4.13: Badal system between the two lenses of the last telescope. By moving the two combined prisms on the left, the optical path between the two lenses can be extended or shortened. This can be used to compensate defocus of a subject's eye.

The system's stage, on which the two prisms on the left in Fig. 4.13 are mounted, should be in a central position, to allow maximum travel range

in both directions. Then the alignment mirror has to be removed. At next the light beam should be centered on the first prism and the reflected beam should emerge in vertical direction. The light hits the second prism and is reflected into a horizontal direction where it hits the third prism. Here the beam is reflected again in horizontal direction but this time out of the plane spanned by the three prisms. With this configuration the height of the beam is changed in order to match the height of the subject's eye during measurement.

The alignment is an easy task using the infra-red sensor cards, but it's important to hit each prism at the center of its reflecting surface. Otherwise, when using large scanning angles, the light beam could be cut off by the edge of the prism. Now the alignment mirror must be placed at the approximate position, of the patient's eye. The mirror is used to reflect the light back through the system.

To continue the first lens of the first telescope must be put into the setup again. Now the last lens must be aligned. With a measuring tape the lens is placed at a distance of 530 mm to the first lens of this telescope. The fine positioning is done with the help of the SH-sensor Zernike bar plot. Iteratively tilts and defocus must be reduced until the defocus is smaller than or equal to  $0.01\mu\text{m}$ . Now the quarter-wave plate can be put at its final position, i.e. in front of the eye. When the signal is centered on the wave front sensor and the signal is not cut off by the aperture the telescope alignment is finished.

## 4.10 Alignment of the detector collimator

The detector collimator must be placed in the detection arm of the setup. It should be placed at the same distance from the first lens as the SH-sensor as shown in Fig. 4.14. Since the pellicle diverts 8 % of the power to the SH-sensor the remaining 92 % can enter the detector collimator and are directed to the APD by a SM-fiber.

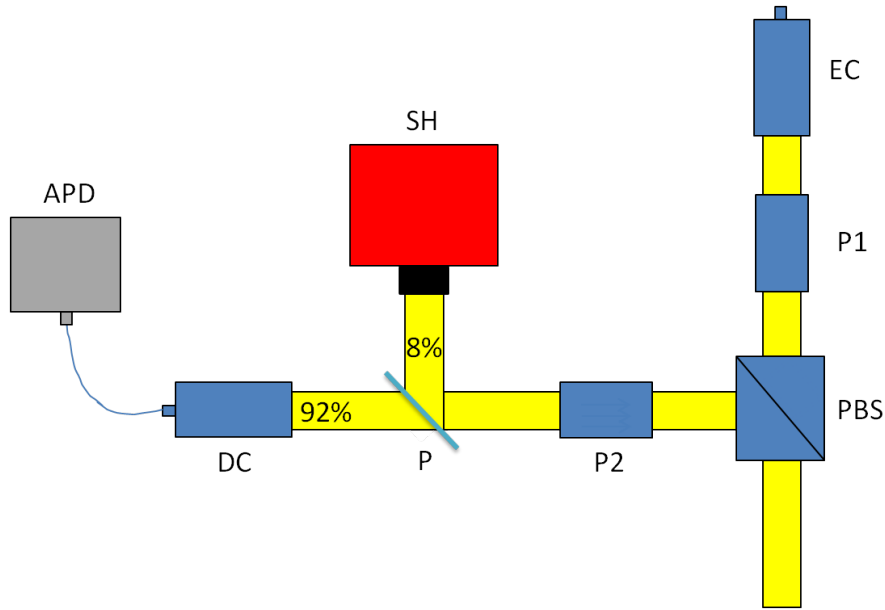


Figure 4.14: Detection arm with installed detector collimator. The collimator couples the light into a SM-fiber which directs the light to the APD, where it is detected. EC...entrance collimator, P1...polarizer 1, PBS...polarizing beam splitter, P2...polarizer 2, P...pellicle, SH...SH wave front sensor, DC...detector collimator, APD...avalanche photo diode

Since a SM-fiber is used it is necessary to couple the light into the fiber. The collimator is mounted on a two-axis stage, allowing to adapt the collimator's height and its position perpendicular to the light propagation direction. On that stage a collimator holder is mounted enabling the possibility to adapt tip and tilt of the collimator. At first the collimator must be put in a position that the light beam hits its lens at the center. Then tip and tilt must be adapted till a spot is visible on an infra-red sensor card held at the back focal plane of the collimator (SM-fiber is disconnected from the collimator). If done so tip and tilt are close to the position at which the light couples into the SM-fiber. In a next step the fiber is connected to the collimator. By systematically searching with a powermeter connected to the other end of the fiber within a narrow range around these tip and tilt it should be easy to find the position where a maximum of light power is coupled in. The light power can further be maximized by adapting height and the position perpendicular to the light propagation direction. After this the setup is ready for measurements.



## 4.11 Problems with the alignment

The alignment of an AO-SLO is a time consuming task. High accuracy is necessary and little mistakes or short negligence may force to start the alignment from the beginning.

One problem when first aligning the system is not to know how accurate the alignment can be achieved. Since the wave front sensor allows to measure the Zernike coefficients very precisely a little improvement is always possible. Even when a defocus coefficient of  $0.01\text{ }\mu\text{m}$  is reached, a further reduction is possible, but very time consuming. For this work, the whole setup was aligned three times.

Another problem is astigmatism. Although the telescopes following the Galvo scanner were built and aligned very often, a non negligible amount of astigmatism could be measured from this point on. Aberrations due to diffraction may be excluded as cause because the scanner head is 11 mm in diameter and the light beam has a diameter of 8 mm. A similar problem occurred at the resonant scanner. After this scanner a spherical aberration was measured and couldn't be removed.

Another problem is caused by the DM. After aligning it's position the defocus measured was not zero. After eliminating some other possible sources for the defocus the DM was found to cause the defocus. This was found out by simply putting the alignment mirror in front of the DM. In that case the defocus was nearly zero as expected. When removing the mirror a defocus was measured. The problem is that the DM shows drift (c.f. Fig. 3.5). Within two hours the defocus triples. This drift causes problems when aligning the system (during AO-operation the shape of the mirror will be dynamically changed and this effect doesn't occur). In order to align the system, a command was sent to the DM which should set the DM to "flat". However, this state is maintained only for one minute. During this minute the alignment can be carried out. After this, the DM has to be set into its default shape and after that it can be set to flat again (for another minute). This problem makes the alignment procedure rather time consuming.

# Chapter 5

## Adaptive optics loop control using Matlab[33]

This chapter describes how to drive the AO loop with Matlab. First some prearrangements will be presented and then it is outlined how to close the loop.

### 5.1 Introduction

In the setup an Optocraft SH-sensor and an Alpao DM are used. Alpao also supplies the Alpao Core Engine (ACE) enabling customers to adapt the AO loop's algorithms to their distinct requirements. Since the ACE is implemented in object oriented Matlab code the user can derive classes from supplied classes and overwrite different class methods to his needs.

The main Matlab scripts to initiate the SH-sensor and the DM were provided by Alpao and can be found in the appendix.

### 5.2 Prearrangements

After installation of the SH-sensor, the DM and the ACE (as described in the manual) the user can proceed with starting the ACE. For this purpose the `userStartup.m` (see A.1) Matlab script must be executed by typing the following command:

```
userStartup
```

This script initiates the wave front sensor and the DM. For the SH-sensor the size of the circular mask used for spot detection is defined. For the SH-sensor as well as the DM calibration files are loaded. A Matlab loop object

is created and SH-sensor and DM are included to the loop object. At next the loop object is set to online mode. This means the loop object can be used for closing the AO loop. Finally the data integration time (DIT) is set to 24000  $\mu$ s and the wave front reconstruction mode is set to modal. Now the signal on the wave front sensor can be plotted by typing the following command:

```
wfs.StartRtd
```

This opens the real time display shown in Fig. 5.1.

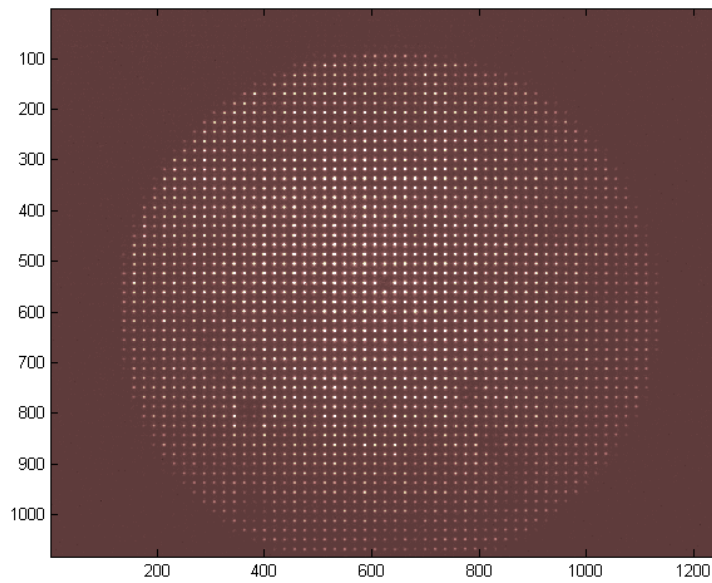


Figure 5.1: The SH-sensor's real time display

In the case the sensor is overexposed or not enough light gets to the sensor chip the real time display will be very bright or black. The DIT needs to be adapted by typing

```
wfs.dit=x;
```

where for x a number between 20  $\mu$ s and 24000  $\mu$ s can be chosen until the two dimensional spot pattern can be seen clear on the real time display figure. The number of bad spots can be displayed with the following command:

```
wfs.StartSlopeRtd
```

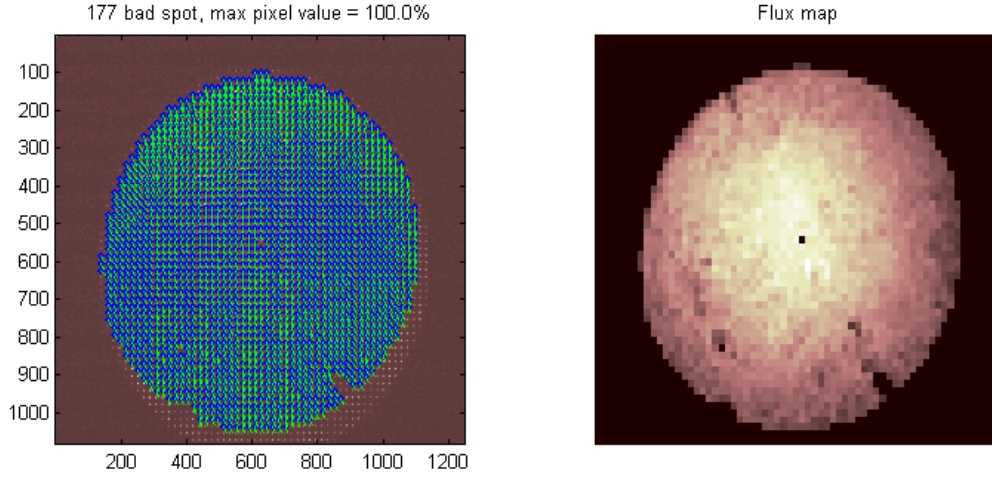


Figure 5.2: Calculated wave front slopes and flux map from SH-sensor data.

A new window displaying the calculated wave front slopes (c.f. Fig. 5.2) is opened. Now the DIT can be adjusted to minimize the number of bad spots.

After this prearrangements the interaction matrix of the AO-system must be recorded. The interaction matrix contains the information how each of the actuators of the DM influences the wave front (c.f. Fig. 5.3). Equation 5.1 shows the interaction matrix where  $n$  represents the number of actuators of the DM and  $k$  represents the number of micro lenses of the lenslet array within the defined pupil mask[33].

$$IM = \begin{pmatrix} a_{11} & \cdots & a_{1n} \\ \vdots & \ddots & \vdots \\ a_{k1} & \cdots & a_{kn} \end{pmatrix} \quad (5.1)$$

Each of the coefficients  $(a_{11} \cdots a_{kn})$  contains the slopes in x and y directions for one micro lens if one actuator is poked[33].

To get a good interaction matrix it is best to place the artificial eye (AE) (consisting of an aperture and a lens with a focal length of 30 mm in front of a black paper simulating the human eye) approximately at the position where later the human eye will be and turn scanning on. With scanning local variances in the backscattered intensity from the modal eye are eliminated because the SH-sensor integration time is much longer then the time of a line scan. The interaction matrix is essential to calculate the command matrix which contains the information how the actuators must be driven to set

different wave front forms (distinct Zernike modes) to the DM. To record the interaction matrix the calibration cell in LOOPscript.m (see A.2) must be executed.

This cell of the LOOPscript.m tells the DM to push and pull each actuator nAverage times with 20 % of the maximum push/pull. For each actuator the corresponding wave front of the pushes and pulls are measured with the SH-sensor, averaged and recorded.

Recording the interaction matrix lasts some minutes, depending on the values set for nAverage and nbPushPull. To avoid recording of a new interaction matrix whenever the loop is closed the interaction matrix can be saved using the following command, in which 'im160712.mat' is the designated file name:

```
loop.SaveMatrix('im160712.mat');
```

## 5.3 Closed loop control

After recording the interaction matrix the loop can be closed. A saved interaction matrix can be loaded with the LoadIMScript.m (see A.3):

```
LoadIMScript
```

This script loads a saved interaction matrix (before execution it needs to be edited so that the name of the desired saved interaction matrix is given the LoadMatrix command). After loading the interaction matrix the script opens the real time display plot and the mirror monitoring plot. Then the script excludes tip and tilt from wave front reconstruction and correction. The rest of the first 60 Zernike modes are used for reconstruction and correction. Then the command matrix is computed out of the interaction matrix, the loop gain factor set to 0.5 and the loop is closed.

The loop can be opened again by executing the following commands:

```
loop.Open;           % open loop
dm.Reset;            % reset mirror
```

It can be interesting to plot the influence function. This can be done by executing the following command:

```
loop.drawIF;
```

This opens a plot shown in Fig. 5.3 in which the influence of each actuator on the wave front can be seen.

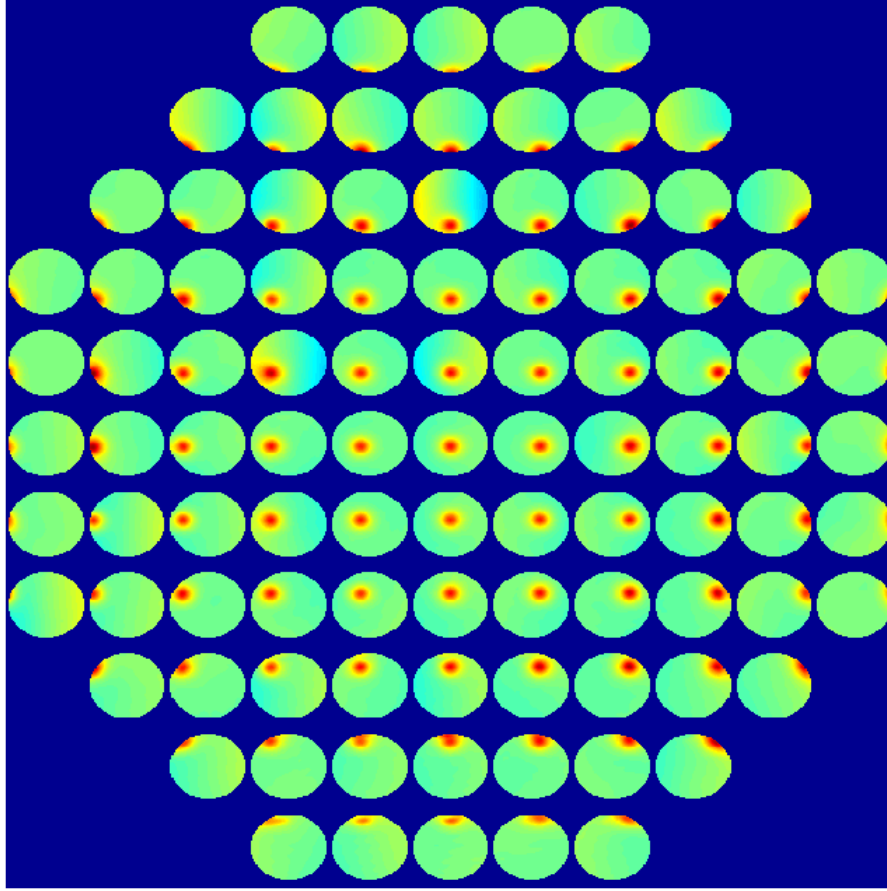


Figure 5.3: Plot of the influence function. Each circle corresponds to the influence of one DM element on the wave front.

Sometimes it can be necessary to close the AO loop and then freeze the DM in its last shape. This can be done by closing the loop with the previous scripts and then executing the following command:

```
loop.Open;
```

Figure 5.4 shows different parameters after closing the AO-loop. The RMS reduces to a 10th of the initial value. In the wave front plot in the left upper corner the DM's regular actuator grid can be seen.

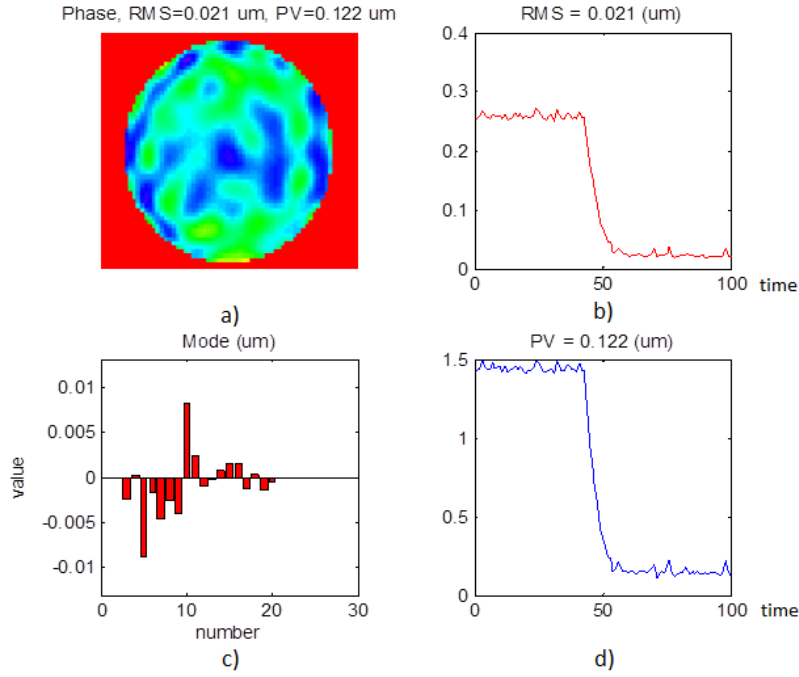


Figure 5.4: Different parameters during closing of AO-loop. a) wave front, b) RMS of the wave front, c) Zernike modes of the wave front, d) Peak to valley (PV) of the wave front.

In order to observe the status of each actuator a mirror monitor plot is provided by the software. An example is shown in Fig. 5.5. Each actuator and its driving signal is shown on a color scale. The max command value above the plot shows the latest maximum driving command. This plot is very helpful in order to see when an actuator is close to the limit of operation. In a stable running AO closed loop the actuator driving signals should be within a narrow interval and should not change over time.

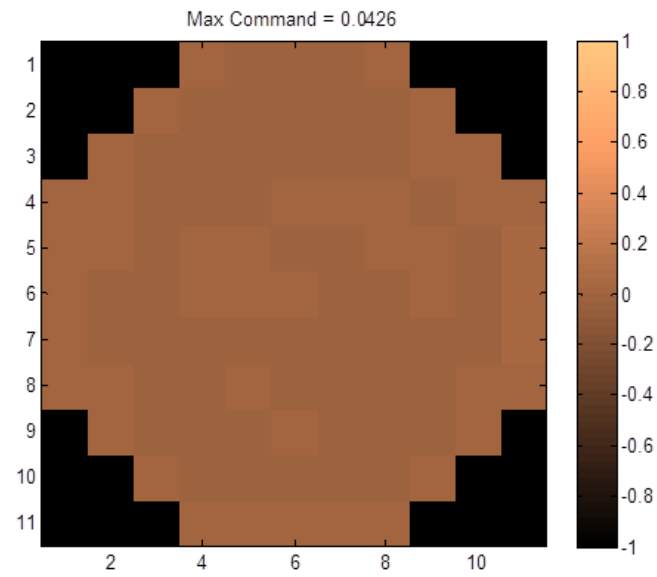


Figure 5.5: Mirror monitor of a closed loop. The max command value is low and stable, which means that the AO closed loop mode runs stable.



## Chapter 6

# System characterization and measurements

During assembly of the instrument a lower sensitivity of the SH-sensor in comparison to a similar instrument [14] was noticed. Therefore a rough estimation of the expected exposure time required for in vivo measurements was performed.

### 6.1 Rough calculation of the required sensitivity of the SH-sensor for in vivo measurements

The allowed power to expose the eye ( $P_{eye}$ ) at the used wavelength (840 nm) is 700  $\mu$ W (without scanning). Assuming that only 1/10000 of the power is back reflected by the eye ( $\gamma_{eye}$ ) high sensitivity is necessary. The maximum possible DIT ( $t_{DIT}$ ) that can be set is 24 ms. The setup reduces the power on the way from the eye to the SH-sensor by 0.5 ( $\gamma_{setup}$ ) and only 8% of the power are diverted for wave front measurement by the pellicle ( $\gamma_{pell}$ ). As a consequence the energy exposing the SH-sensor ( $E_S$ ) can be calculated with Eq. 6.1.

$$E_S = P_{eye} t_{DIT} \gamma_{eye} \gamma_{setup} \gamma_{pell} = 700 \cdot 10^{-6} 24 \cdot 10^{-3} 10^{-4} \cdot 0.5 \cdot 0.08 = 6.7 \cdot 10^{-11} J \quad (6.1)$$

This energy is divided to about 1960 spots ( $N_{spots}$ ) by the lenslet array (2500 micro lenses but only a circular aperture is illuminated by the beam). Each spot extends to about 50 pixel ( $N_{pix}$ ) on the sensor chip. To calculate the Joules per pixel  $E_P$  Eq. 6.2 is used.

$$E_P = \frac{E_S}{N_{spots}N_{pix}} = \frac{6.7 \cdot 10^{-11}}{1960 \cdot 50} = 6.8 \cdot 10^{-16} \frac{J}{Pixel} \quad (6.2)$$

Since  $E = h\nu$  and  $c = \lambda\nu$  the energy of one quantum at a wave length of 840 nm can be calculated with Eq. 6.3, where  $h$  is the Planck constant ( $6.626 \cdot 10^{-34} Js$ ),  $c$  is the speed of light ( $3 \cdot 10^8 \frac{m}{s}$ ) and  $\lambda$  is the wave length (840 nm).

$$E_{840nm} = \frac{hc}{\lambda} = 2.4 \cdot 10^{-19} J \quad (6.3)$$

With the values calculated in Eq. 6.2 and 6.3 the quanta per pixel can be calculated 6.4.

$$N_{quant} = \frac{E_P}{E_{840nm}} = \frac{6.8 \cdot 10^{-16}}{2.4 \cdot 10^{-19}} = 2833 \quad (6.4)$$

The sensor has a quantum efficiency  $\eta$  of 0.5 so the number of collected electrons is  $\sim 1416$ . The sensor is an 8 bit sensor with a full well capacity of 500000  $e^-$  (1 bit corresponds to 1953 electrons). The amount of collected electrons is below the digitation noise. As a consequence the signal is too low when the eye is exposed with the maximum allowed power.

This prevented AO enhanced in vivo measuring in the current configuration. However, it was possible to correct the system aberrations which are in the setup due to residual misalignments. To achieve this an AE was used as sample. At next the power was increased until wave front correction was possible and the loop was closed. After a short time the static system aberrations were corrected and the loop could be opened and the shape of the deformable mirror was fixed in the last shape. Now the power was reduced below 700  $\mu W$  and measurements on the eye of a volunteer were performed.

## 6.2 Measurement of the system sensitivity

The system sensitivity was measured by placing a mirror at the position of the eye. To get the SNR the standard deviation of the SLO signal was measured when the light path was blocked so that no light was sent to the detector. Then the maximum SLO signal was determined after reducing the light power with neutral density filters. This yielded a system sensitivity of 57.4 dB.

### 6.3 Artificial eye and in vivo imaging of a human eye

The AE backreflects more light than the human eye. Moreover, for the AE the power can exceed the limitation of  $700\text{ }\mu\text{W}$  mentioned in the previous section. The power at the AE was  $1.5\text{ mW}$ . As a consequence it was possible to take a measurement of the AE with closed loop. Data was recorded with a sampling rate of  $50\text{ MS}$  and the total recording time of 30 frames was 3 seconds (recording speed was  $10\text{ fps}$ ). Figure 6.1 shows a typical image of the AE. The wave front when measuring the AE is shown in Fig. 6.2.

To get the SNR when measuring the artificial eye the above measured standard deviation was used. Then the maximum SLO signal was determined when the AE is illuminated with  $175\text{ }\mu\text{W}$ . The APD was saturated for this illumination power so a  $13\text{ dB}$  filter was added to the setup causing a decrease in SNR of  $26\text{ dB}$  (the light traverses the filter twice). The SNR was calculated with Eq. 2.8 to  $17.3\text{ dB}$ . Using only  $175\text{ }\mu\text{W}$  instead of  $700\text{ }\mu\text{W}$  commensurates to a SNR loss of  $6\text{ dB}$ . By adding up the calculated SNR, the filter loss and the  $6\text{ dB}$  for using only  $175\text{ }\mu\text{W}$  the SNR of the AE image was calculated resulting to  $49.3\text{ dB}$ . Therefore the light is attenuated by the AE by  $8.1\text{ dB}$ .

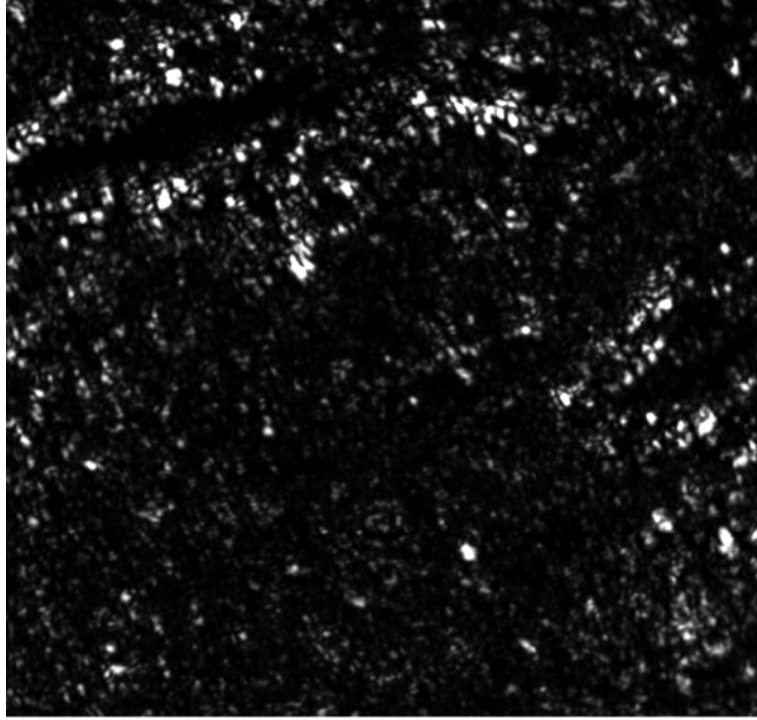


Figure 6.1: AO-SLO image of the AE. Image size:  $1^\circ \times 1^\circ$

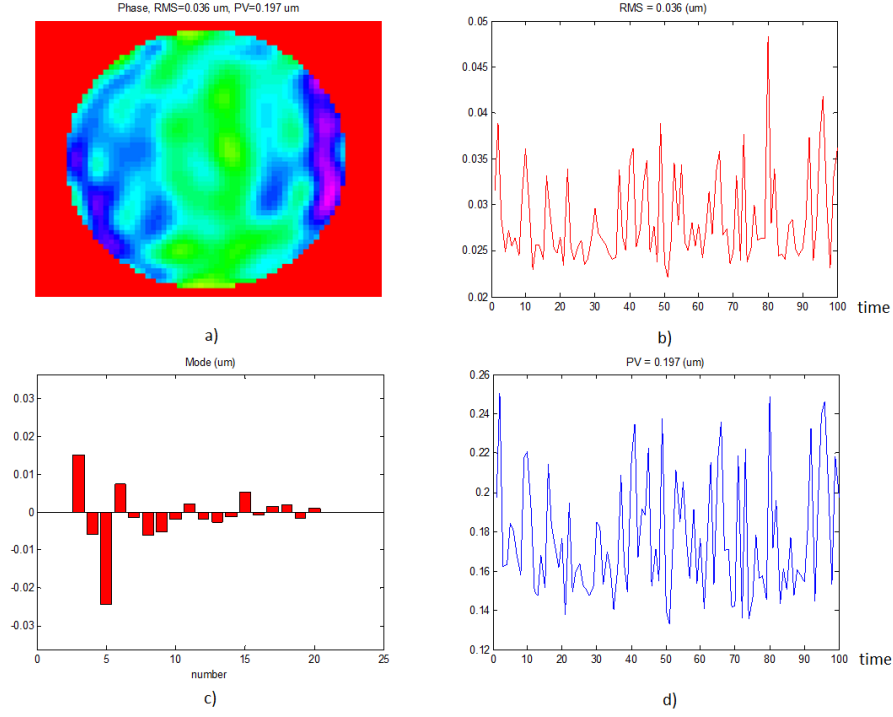


Figure 6.2: Corrected wave front when measuring the AE: a) wave front, b) RMS of the wave front, c) Zernike modes of the wave front, d) PV of the wave front.

Figure 6.3 shows two scans of the AE. The left scan was performed without AO while for the right scan the AO loop was closed for a short time (about one second) and then the DM was kept in the latest shape. By this the RMS for the right scan was reduced to a third of the initial RMS of the left scan (about  $0.8\mu\text{m}$ ). Due to system aberrations and aberrations introduced by the AE, the improvement in signal quality is not much pronounced.

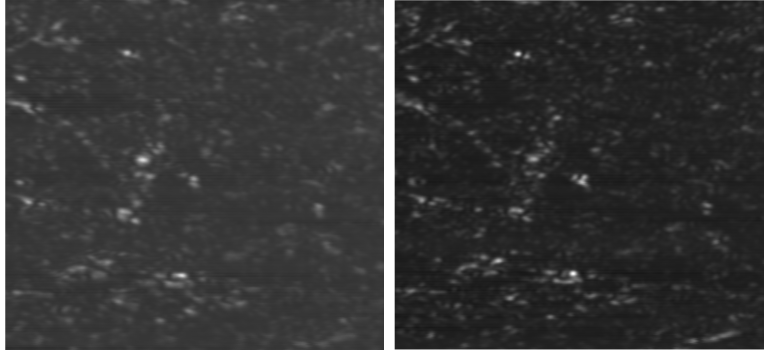


Figure 6.3: The left image shows a scan of the AE without AO. For the right image the AO loop was activated for a short time (about one second) and then the DM was frozen in the latest shape. The RMS in the right image is about a third of the RMS in the left image (about  $0.8\text{ }\mu\text{m}$ ).

To test the performance of the system for in vivo imaging the incident power was reduced below  $700\text{ }\mu\text{W}$ . All measurements were performed under a protocol that was approved by the ethics committee of the Medical University of Vienna and which followed the tenets of the Declaration of Helsinki. Since AO-closed loop operation could not be achieved for in vivo imaging (c.f. previous chapter), measurements were taken after residual system aberrations were corrected. In Fig. 6.4 first in vivo measurements of the new AO-SLO system on a healthy volunteer are presented. Although aberrations were only corrected for the system itself the cone mosaic (individual photoreceptors) could be resolved. The image consists of  $5402 \times 620$  pixel and covers an area of  $1^\circ \times 1^\circ$  on the retina. The eye length of the subject ( $18.96\text{ mm}$ ) was measured with an IOLMaster 500 from Zeiss. This allows calculating the scanning area to about  $331\text{ }\mu\text{m} \times 331\text{ }\mu\text{m}$ . The image was recorded at about  $3^\circ$  eccentricity nasal to the fovea.

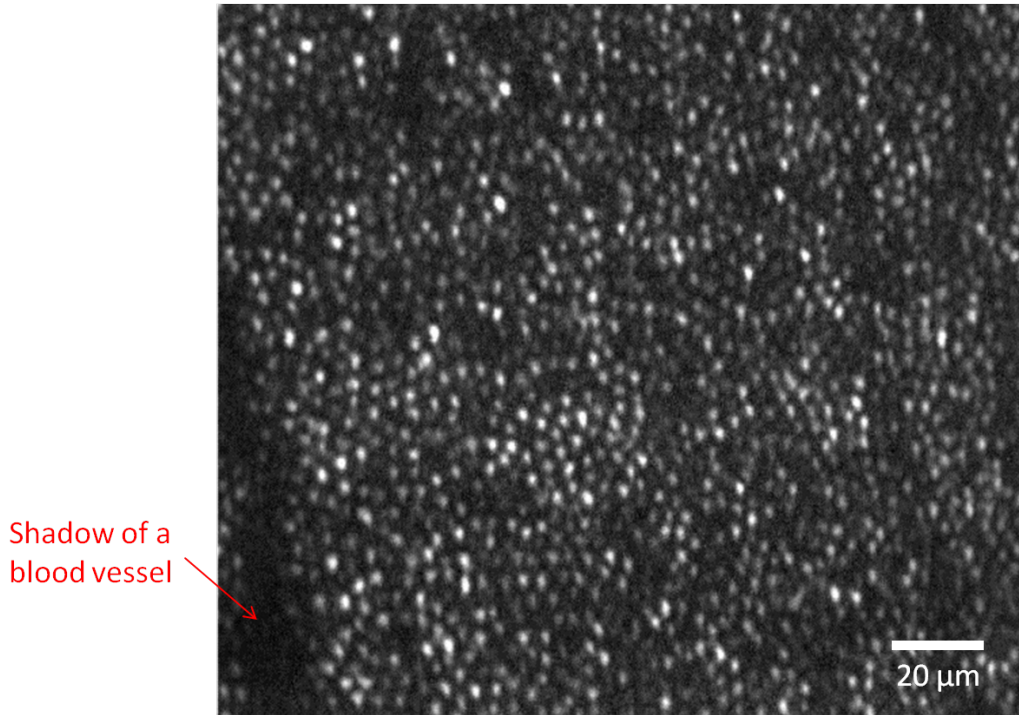


Figure 6.4: First measurements of the cone mosaic of a human eye in vivo. Scanning area about  $1^\circ \times 1^\circ$  ( $331 \mu\text{m} \times 331 \mu\text{m}$ ), located at about  $3^\circ$  eccentricity from the fovea.

In order to quantify the cone to cone spacing Fast Fourier Transform (FFT) can be used[34]. Fig 6.5 shows the FFT of Fig. 6.4. Because of the regular spacing of the cones, Yellott's ring can be observed[35]. The radius of the ring corresponds to the row to row spacing which can be converted into closest neighbour spacing via multiplication by  $(1/\cos 30^\circ)$  [35]. With a radius of 70 pixel a closest neighbour spacing of  $5.5 \mu\text{m}$  was calculated. Assuming a hexagonal spacing of the cones, a cone density of about 33000 cones/ $\text{mm}^2$  can be calculated which is in good agreement with values at this eccentricity obtained from histology[35][36].

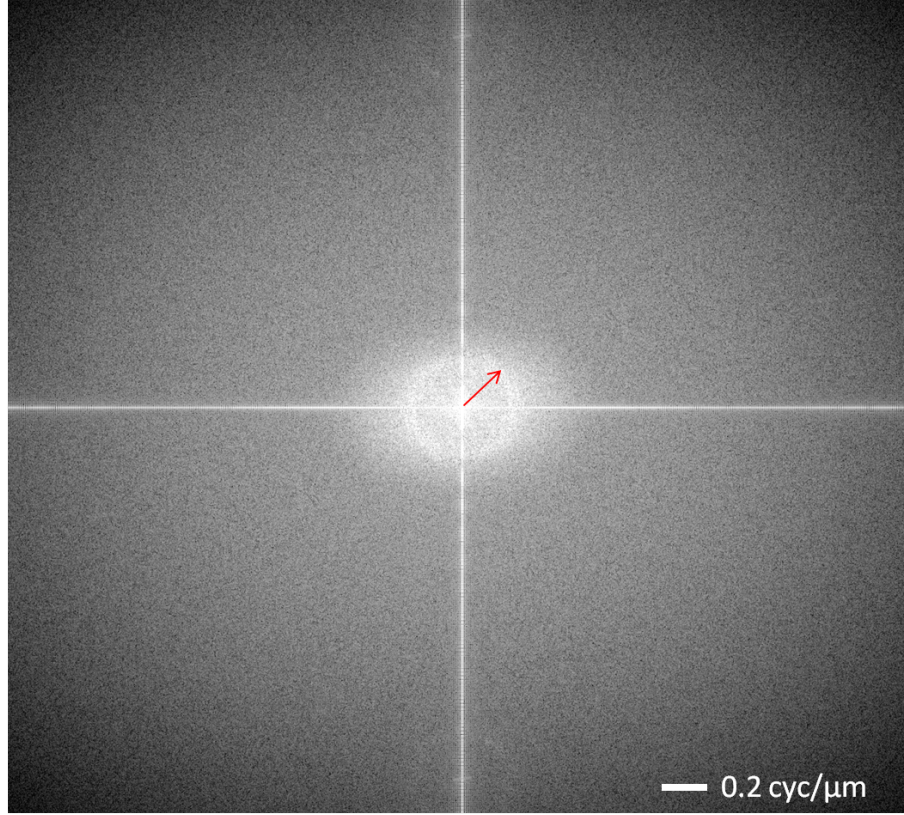


Figure 6.5: FFT of the cone mosaic in Fig. 6.4. The radius (red arrow) of the circle in the center of the image allows assessing the cone density.

Finally the signal to noise ratio (SNR) of the in vivo image is determined. The standard deviation of the detector noise was measured with  $\sim 76$ . For the original image (c.f. Fig. 6.4) the maximum signal was measured ( $\sim 32000$  a.u.). This yields a SNR of  $\sim 26$  dB of the image.



# Chapter 7

## Discussion and outlook

For this thesis a complete lens based AO-SLO setup was built and aligned. At first the basic principles of SLO and AO were presented. Then the different devices contained in the lens based AO-SLO setup were described. In a next step a detailed insight into the alignment of a lens based AO-SLO was given. After the alignment procedure the software control of the AO loop was described. Finally measurements of an artificial eye and a human volunteer in vivo were presented. The human cone mosaic could be resolved at an eccentricity of  $\sim 3^\circ$  nasal from the fovea. The cone density was calculated and corresponded well to values known from histology. These high resolution images were possible because the subjects aberrations were low.

However, because of the low sensitivity of the SH-sensor it was not possible to tap the full potential of the setup. The low light powers required for save illumination of the human eye were insufficient for a reasonable signal on the SH-sensor. As a consequence it was not possible to correct the wave front aberrations for the in vivo measurements. Only the system aberrations could be corrected prior to the in vivo measurement with the AO loop.

One approach to solve this problem is to adapt the software to adding several SH-sensor images which corresponds to an increase of the DIT. However, this approach did not solve the problem because it slowed down the AO-loop. This is caused by the relative high readout time of the SH-sensor. Therefore, in vivo measurements were not meaningful with this approach. Another approach could be to replace the pellicle with a pellicle that diverts 50% of the power for wave front measurement instead of only 8%. However, in this case light for imaging is sacrificed.

To realise the full potential of the setup the SH-sensor has probably to be replaced with a wave front sensor with higher sensitivity.

Furthermore, to enable measuring 3D tomograms of the retina the setup can be implemented into an optical coherence tomography (OCT) setup

[11][12] as sample arm. Once the problem with the SH-sensor is solved the system may be adapted for patient imaging. This step requires the implementation of a fixation target and an additional anterior segment monitor.

# Bibliography

- [1] D. Miller, O. Kocaoglu, Q. Wang, and S. Lee, “Adaptive Optics and the Eye,” *Cambridge Ophthalmological Symposium* **25**, 321–330 (2011).
- [2] N. Bressler, S. Bressler, and S. Fine, “Age-related Macular Degeneration,” *Survey of Ophthalmology* **32**, 375–413 (1988).
- [3] F. Grehn, *Augenheilkunde* (Springer Medizin Verlag, 2007).
- [4] S. Choi, N. Doble, J. Hardy, M. Steven, J. Keltner, and S. Oliver, “In vivo imaging of the photoreceptor mosaic in retinal dystrophies and correlations with visual function.” *Investigative Ophthalmology & Visual Science* **47**, 2080–2092 (2006).
- [5] J. Wolfing, M. Chung, J. Carroll, A. Roorda, and D. Wi, “High resolution imaging of cone-rod dystrophy,” *Ophthalmology* **113**, 1014–1019 (2006).
- [6] A. E. Elsner, “Fundamental Properties of the Retina,” in *Adaptive Optics for Vision Science*, J. Porter, H. M. Queener, J. E. Lin, K. Thorn, and A. Awwal, eds. (John Wiley & Sons, Inc., 2006), pp. 205–234.
- [7] M. Pircher, B. Baumann, E. Götzinger, H. Sattmann, and C. K. Hitzenberger, “Simultaneous SLO/OCT imaging of the human retina with axial eye motion correction,” *Optics Express* **15**, 16 922–16 932 (2007).
- [8] J. Porter, H. M. Queener, J. E. Lin, K. Thorn, and A. Awwal, *Adaptive Optics for Vision Science* (John Wiley & Sons, Inc., 2006).
- [9] S. Schmitz-Valckenberg, F. G. Holz, and A. C. Bird, “Fundus Autofluorescence Imaging - Review and Perspective,” *Retina - The Journal of Retinal and Vitreous Diseases* **28**, 285–409 (2008).
- [10] R. Webb, G. Hughes, and F. Delori, “Confocal Scanning Laser Ophthalmoscope,” *Applied Optics* **26**, 1492–1499 (1987).

- [11] A. Fercher, W. Drexler, and C. Hitzenberger, “Optical Coherence Tomography - Principles and Applications,” *Reports on Progress in Physics* **66**, 239–303 (2003).
- [12] J. Schmitt, “Optical Coherence Tomography (OCT): A review,” *IEEE Journal of Selected Topics in Quantum Electronics* **5**, 1205–1215 (1999).
- [13] J. Liang and D. Williams, “Aberrations and retinal image quality of the normal human eye,” *Journal of the Optical Society of America A-Optics Image Science and Vision* **14**, 2873–2883 (1997).
- [14] F. Felberer, J.-S. Kroisamer, C. K. Hitzenberger, and M. Pircher, “Lens based adaptive optics scanning laser ophthalmoscope,” *Optics Express* **20**, 17 297–17 310 (2012).
- [15] A. Roorda, F. Romero-Borja, W. Donnelly, H. Queener, T. Hebert, and M. Campbell, “Adaptive Optics Scanning Laser Ophthalmoscopy,” *Optics Express* **10**, 405–412 (2002).
- [16] D. Hammer, R. Ferguson, C. Bigelow, N. Iftimia, T. Ustun, and S. Burns, “Adaptive Optics Scanning Laser Ophthalmoscope for Stabilized Retinal Imaging,” *Optics Express* **14**, 3354–3367 (2006).
- [17] A. Dubra, Y. Sulai, J. L. Norris, R. F. Cooper, A. M. Dubis, D. R. Williams, and J. Carroll, “Noninvasive imaging of the human rod photoreceptor mosaic using a confocal adaptive optics scanning ophthalmoscope,” *Biomedical Optics Express* **2**, 1864–1876 (2011).
- [18] R. Ferguson, Z. Zhong, D. Hammer, M. Mujat, A. Patel, C. Deng, W. Zou, and S. Burns, “Adaptive Optics Scanning Laser Ophthalmoscope with integrated wide-field retinal imaging and tracking,” *Journal of the Optical Society of America A-Optics Image Science and Vision* **27**, A265–A277 (2010).
- [19] W. Demtröder, *Experimentalphysik 2, Elektrizität und Optik* (Springer, 2006).
- [20] N. Doble and D. T. Miller, “Wavefront Correctors for Vision Science,” in *Adaptive Optics for Vision Science*, J. Porter, H. M. Queener, J. E. Lin, K. Thorn, and A. Awwal, eds. (John Wiley & Sons, Inc., 2006), pp. 83–118.
- [21] G. Yoon, “Wavefront Sensing and Diagnostic Uses,” in *Adaptive Optics for Vision Science*, J. Porter, H. M. Queener, J. E. Lin, K. Thorn, and A. Awwal, eds. (John Wiley & Sons, Inc., 2006), pp. 63–82.

- [22] Optocraft, *SHSLab Technical manual* (2007).
- [23] Alpao, *Man-Hi-Speed DM97-15-001* (2010).
- [24] S. Cornelissen, T. Bifano, and P. Bierden, “MEMS Deformable Mirror Actuators with Enhanced Reliability,” *MEMS Adaptive Optics VI* **8253** (2012).
- [25] L. Chen, “Control Algorithms,” in *Adaptive Optics for Vision Science*, J. Porter, H. M. Queener, J. E. Lin, K. Thorn, and A. Awwal, eds. (John Wiley & Sons, Inc., 2006), pp. 119–138.
- [26] Superlum, *Acceptance Test Report Device No. 120468* (2005).
- [27] Optocraft, *SHS Works* (2011).
- [28] GSI-Group, *CRS Series Resonant Optical Scanners* (2006).
- [29] Cambridge Technology, *Datasheet Model 6230H Optical Scanner* (2007).
- [30] Laser Components, *APD Module LCSA/LCIA-Series* (2012).
- [31] Alazar Technologies, *ATS9440 User Manual* (2011).
- [32] A. Bradu, A. G. Podoleanu, D. Merino, and C. Dainty, “Design Criteria of an Adaptive Optics - OCT/SLO System,” in *Conference Paper Biomedical Topical Meeting (BIO)* (2006).
- [33] Alpao, *Alpao Core Engine rev 1.3* (2012).
- [34] J. Yellott, “Spectral analysis of spatial sampling by photoreceptors: Topological disorder prevents aliasing,” *Vision* **22**, 1205–1210 (1982).
- [35] M. Pircher, R. Zawadzki, J. Evans, J. Werner, and C. Hitzenberger, “Simultaneous imaging of human cone mosaic with adaptive optics enhanced scanning laser ophthalmoscopy and high-speed transversal scanning optical coherence tomography,” *Optics Letters* **33** (2008).
- [36] C. Curcio, R. Sloan, R. Kalina, and A. Hendrickson, “Human photoreceptor topography,” *Journal of comparative neurology* **292**(4), 497–323 (1990).

# Appendix A

## Matlab scripts

### A.1 userStartup

```
%% Deformable mirror
wfs = aceptocraft150SHS();
% create a wave front sensor object
[X,Y] = meshgrid(linspace(-1, 1, 57));
smask = (sqrt(X.^2+Y.^2)<=0.95);
mask = zeros(66, 57);
mask(5:61, :) = smask;
mask = acewfsMASK(mask);
wfs.set('sMask', mask); % set circular mask
wfs.serialFile = '0111101064_840nm_1248x1082pixel.par';
% load SH-sensor serial file to initialize
% the wave front sensor
acegui.wfs = wfs; % add created wave front sensor
% object to ACE
%% Deformable Mirror
disp('Build Deformable Mirror...');
dm = acewfcMAG_DM97('alpaoHSDM97-15-043');
% create deformable mirror object and initialize it with
% calibration data, set deformable mirror in online mode

%% LOOP
disp('Build Loop...');
loop = aceloopLOOP(); % create loop object
acegui.wfs = wfs;
% add wave front sensor object to ACE
acegui.dm = dm;
% add deformable mirror object to ACE
```

```

acegui.loop = loop;      % add loop object to ACE

loop.set('sWfc', dm);
% attach deformable mirror to loop object
loop.set('sWfs', wfs);
% attach wave front sensor to loop object
loop.Online      % set loop in online mode
loop.closeLoopThread.sleepTime = 50;
wfs.dit = 24000; % set data integration time to
% 24000 micro seconds
wfs.sReconstructor.type = 'modal';
% set wave front reconstruction mode

```

## A.2 LOOPScript

```

%% Calibration
loop.interactionMatrix = [];
% set interaction matrix to zero
loop.influenceMatrix = [];
% set influence matrix to zero
loop.commandMatrix = [];
% set command matrix to zero
nAverage = 8;
% set number of measurements to average
% over for each actuator
nbPushPull = 1;
% set number of pushes/pulls for each actuator
loop.BuildIM(0.02, nAverage, nbPushPull);
% start influence matrix measurement:
% each actuator is set a
% driving signal of 0.02 nbPushPull-times
% and it is averaged over
% nAverage measurements
loop.sWfc.Reset();
%% (re)Build
loop.nModes = 60;
% the first 60 modes are used for adaptive optics
loop.BuildCM(); % build command matrix
loop.gain = 0.5; % loop gain factor
%% Monitor
wfs.StartWavefrontRtd;

```

```

% start the wave front real time display
dm.StartMonitoring
% start deformable mirror monitoring
%% Close Loop
loop.Close;      % close the loop

```

### A.3 LoadIMScript

```

%% Close loop after loading new interaction matrix
loop.LoadMatrix('im160712.mat') % load interaction matrix
wfs.StartWavefrontRtd; % start wave front real time display
dm.StartMonitoring; % start deformable mirror monitoring
pause(1); % pause one second
wfs.sReconstructor.validModes(1:2)=0;
% ignore tip and tilt for wave front reconstruction
wfs.filterTilt=1; % ignore tilt for wave front correction
wfs.filterTip=1; % ignore tip for wave front correction
loop.nModes = 60;
% use first 60 modes for wave front correction
% without tip/tilt
loop.BuildCM(); % build command matrix
loop.gain = 0.5; % loop gain factor
loop.Close; % close loop

```